AD NUMBER
AD868280
LIMITATION CHANGES

TO:

Approved for public release; distribution is unlimited.

FROM:

Distribution authorized to U.S. Gov't. agencies and their contractors; Critical Technology; MAR 1970. Other requests shall be referred to Office of Naval Research, code 421, Washington, DC 20360. This document contains export-controlled technical data.

AUTHORITY

onr notice, 27 jul 1971

ADVANCED CAPABILITY INFRARED RECEIVER SYSTEM

FINAL REPORT
(15 March 1968 to 15 December 1969)

March 1970

by

F. Pace, R. Lange, F. Arams, B. Peyton, and E. Sard

AIL Report 3481-F

Prepared Under Contract N00014-68-C-0273

ARPA Order No. 306

Project Code 7E20K21

for

Office of Naval Research
Washington, D.C.
Code - 421
by

AIL, a division of Cutler-Hammer
Deer Park, New York 11729

ADVANCED CAPABILITY INFRARED RECEIVER SYSTEM

FINAL REPORT
(15 March 1968 to 15 December 1969)

March 1970

by

F. Pace, R. Lange, F. Arams, B. Peyton, and E. Sard

ACKNOWLEDGMENT

ii

TABLE OF CONTENTS

LIST OF ILLUSTRATIONS

I. INTRODUCTION AND SUMMARY

This is the final report on a program having as its objective the feasibility demonstration of a 10.6-micrometer coherent heterodyne-receiver array with:

- 3 x 3 (9 elements) mixer configuration

- 1.5-GHz instantaneous IF bandwidth

- Sensitivity near the theoretical quantum noise limit

- Adjacent receiver antenna beam pattern crossovers at -3 dB

This report includes:

- Highlights of the results given in the first semiannual report (reference 1)

- Covers in detail work done in the period from October 1968 to December 1969

- Presents conclusions

The initial investigation proceeded along two paths:

- Development of the coherent array

- Development of the high-performance mixer elements

The results obtained here were then integrated to yield an array technology that meets the program objectives and may be used for larger arrays at least up to a 10 x 10 configuration.

The coherent array development was concerned with the analysis and synthesis of the combined optical fields of the received signal and local oscillator beams. This was followed by detailed optical pattern measurements.

Several methods of forming the array of desired beam patterns were then considered and an array of microlenses (called the image dissector) was selected,

1

fabricated, and tested. The key parameters here were the size and spacing of the micro-lenses and mixer elements with respect to a focused spot of the received signal.

A method for mounting the mixer elements in registration with the beam-forming array of microlenses was devised. It includes such features as microstrip cabling for the microwave IF signal, adequate heat transfer for the mixer elements, and electrical isolation greater than 30 dB over the entire IF bandwidth. The heat transfer of the mixer elements is important because of the additional local oscillator and bias power requirements above that of more conventional infrared detectors.

The mixer development consisted of an extension to 1.5-GHz instantaneous bandwidth of the wideband high-sensitivity technology of photoconductive copper-doped germanium mixers that had been developed on other programs (references 2, 3, and 4). In addition other materials with potential for meeting the program objectives were examined. An in-depth analysis of photovoltaic mixing in 10.6-micrometer intrinsic detector materials, such as mercury cadmium telluride, point to the possibility of good performance at a future date when device fabrication techniques are improved.

Coherent heterodyne reception in infrared radar systems offers several substantial operational improvements over the more conventional infrared envelope (video) detection receiver:

- **Substantially Better Sensitivity.** Heterodyne receiver sensitivity approaches the quantum noise limit (2×10^{-20} watt/Hz at 10.6 micrometers) while envelope detection is orders of magnitude less sensitive ($\approx 10^{-13}$ watt/Hz$^{1/2}$, depending on background temperature and field of view). This represents a very substantial increase in radar range attainable for a given transmitter power.

- **Preserves Frequency and Phase.** Heterodyne reception preserves the frequency and phase of the target return signal, thereby permitting the extraction of doppler (range rate) and target scintillation signature, and the coherent processing of multiple signals at a convenient IF (intermediate frequency). These properties can be key elements in discriminating against reentry decoys.

2

- **Excellent Background Discrimination.** The heterodyne receiver is not affected by normal background levels (including direct sunshine) at 10.6 micrometers. This is due to the extremely narrow (relatively speaking) predetection bandwidth of the receiver and the low spectral density of thermal sources.

- **Good Spatial Discrimination.** The heterodyne receiver element does not respond to stray signals that are not critically aligned with its local oscillator both spatially and in polarization. Such phenomena as scatter side lobes induced by dust or imperfections in the system optics do not affect the spatial discrimination of a heterodyne receiver as readily as that of an envelope detector.

- **Low ECM Vulnerability.** Heterodyne reception is inherently less vulnerable to hostile ECM or unintentional RFI radiations by virtue of its narrow predetection bandwidth, polarization discrimination, and improved spatial discrimination.

In addition to the advantages accruing from the use of coherent heterodyne detection, this array approach to CO_2 laser radar receiver design offers substantial improvements that include:

- **Expanded Instantaneous Field of View Without Loss of Spatial Resolution.** Acquisition is reduced in inverse proportion to the solid angle of the expanded field of view. Tracking capability is enhanced by the additional number of resolution elements. This array receiver is also better matched to the laser transmitter beam which may use smaller optics or be broader than the single-mode diffraction limit.

- **Ability to Resolve Multiple Targets Within Expanded Field of View.** It has been shown that within the same range-doppler-azimuth-elevation resolution cell, all the coordinates of multiple targets can be resolved according to the following schedule:

Number of Array Elements (or Beams)	Maximum Number of Targets
4 (2 × 2)	2
9 (3 × 3)	4
16 (4 × 4)	8
25 (5 × 5)	12

- **Monopulse Capability.** Coherent summing of the individual mixer outputs could result in receiver performance equivalent to that obtained with an optimally designed single-element receiver. This is not the case for a mosaic of envelope detectors.

- <u>Relatively Small Increase in System Cost.</u> This is because common optics and cooling are used.

- <u>Extendable</u> to larger number of array elements.

4

II. ARRAY DEVELOPMENT

A. OPTICAL PATTERN SYNTHESIS

Synthesizing the far-field diffraction pattern for a coherent optical array involves a departure from long-wavelength antenna procedures in that the optical array pattern is strongly affected by the phase-front of the reference or local oscillator beam, which must be included in the design. The array design requires nine identical signal beams, squinted with respect to one another, with crossovers at -3 dB points between adjacent beams.

The approach chosen, to achieve such an overall pattern, was to design the local oscillator beam to be a plane wave traveling normal to the plane of the array and uniformly irradiating it. Figure 2-1 illustrates this situation. The receiving optics transform wavefront tilt of the signal radiation in the receiving aperture into lateral translation about the optic axis in the image plane. This focused signal is added to the plane-wave (approximate) local oscillator in the image plane.

Expressions are derived in Appendix A for the complex amplitudes (electric fields) of the received signal and the local oscillator at the image plane, for it is here that the mixer element is placed to detect the dynamic interference fringes of the combined signals. To interfere efficiently, the polarization of the two components must be aligned. The analysis assumes that this requirement is fulfilled.

For the case of a plane-wave local oscillator and a signal focused by the receiving aperture, an expression is derived (in Appendix A) that gives the IF signal output from a finite area heterodyne mixer element for various combinations of parameter values. These include wavelength, f/number of the focused signal, physical dimensions of the

5

of the mixer element, and relative position of the mixer element with respect to the focused spot. One form of the expression is given as

$$I_m = C \int_{y_1 - \Delta y}^{y_1 + \Delta y} \int_{x_1 - \Delta x}^{x_1 + \Delta x} \frac{J_1\left\{ \frac{ka}{f}\left[\left(x + x'\right)^2 + \left(y + y'\right)^2 \right]^{\frac{1}{2}} \right\}}{\frac{ka}{f}\left[\left(x + x'\right)^2 + \left(y + y'\right)^2 \right]^{\frac{1}{2}}} dxdy$$

where

I_m = mixer output in response to the integrated signal intensity over its surface

C = proportionality constant

(x_1, y_1) = coordinates of the center of the square mixer

$(2\Delta x, 2\Delta y)$ = dimensions of the square mixer

$J_1\left\{ \ \right\}$ = Bessel function of first kind

$K = \frac{2\pi}{\lambda}$

λ = wavelength

f = frequency

(x', y') = spatial variables in image plane referred to direction of arrival

(x, y) = spatial variables in image plane

6
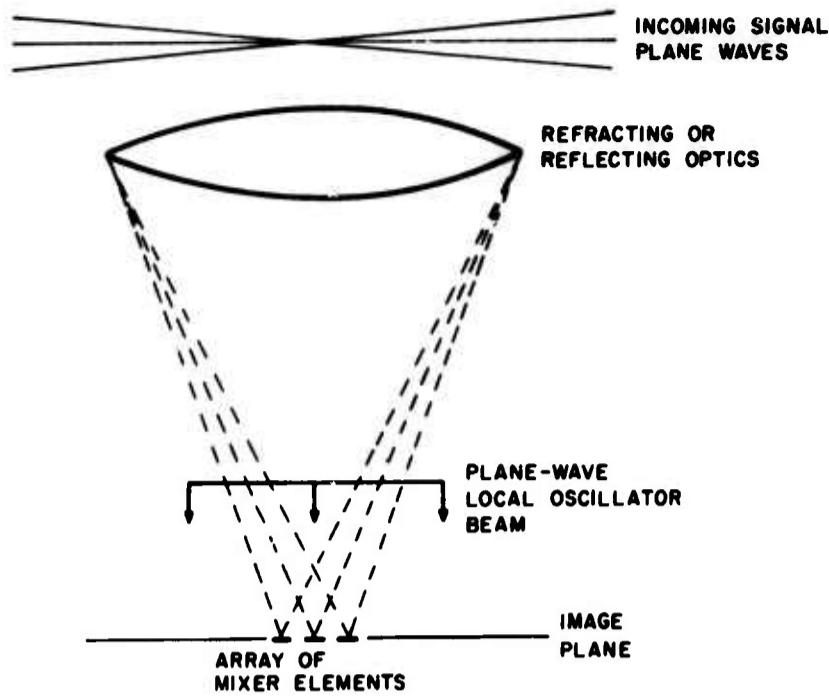
FIGURE 2-1. DIAGRAM OF BEAM-FORMING OPTICS

1.   COMPUTED PATTERNS

By means of a digital computer, values of I_m were computed for several sets of parameter values. When the coordinates of the center of the square mixer (x_1, y_1) are the variables, one obtains the mixer output at various positions in the image plane. This is the diffraction pattern seen by a mixer with finite dimensions. For various size mixers $(\Delta x, \Delta y)$, Figure 2-2 was obtained by sequencing x_1 (in increments of 50 micrometers) with y_1 set equal to zero. The other conditions were:

$$\lambda = 10.6 \text{ micrometers}$$

$$f/number = 10$$

$$2\Delta x = 2\Delta y = 10, \ 50, \ 80, \ 100, \ \text{and } 200 \text{ micrometers}$$

7
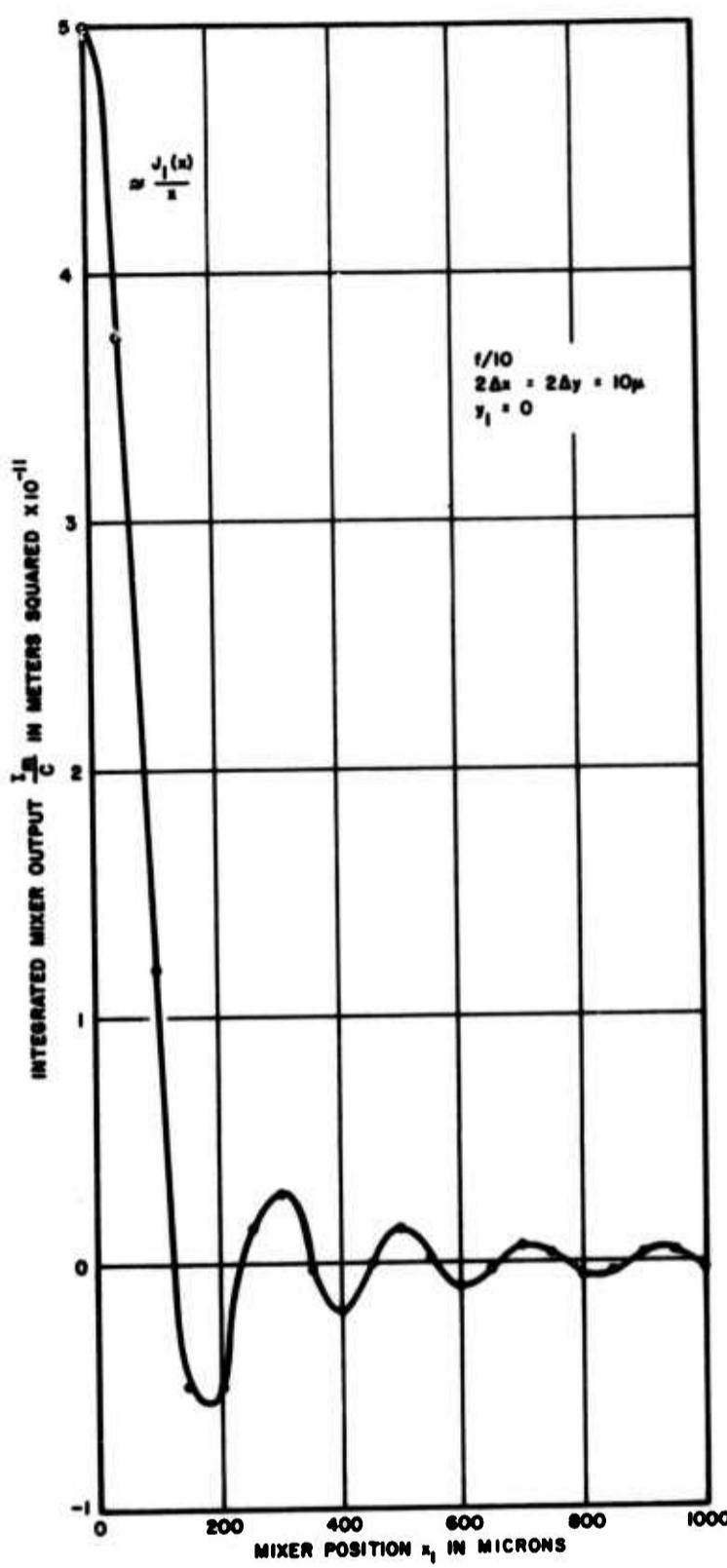
FIGURE 2-2. CALCULATED HETERODYNE RECEIVER BEAM PATTERN (SHEET 1 OF 5)
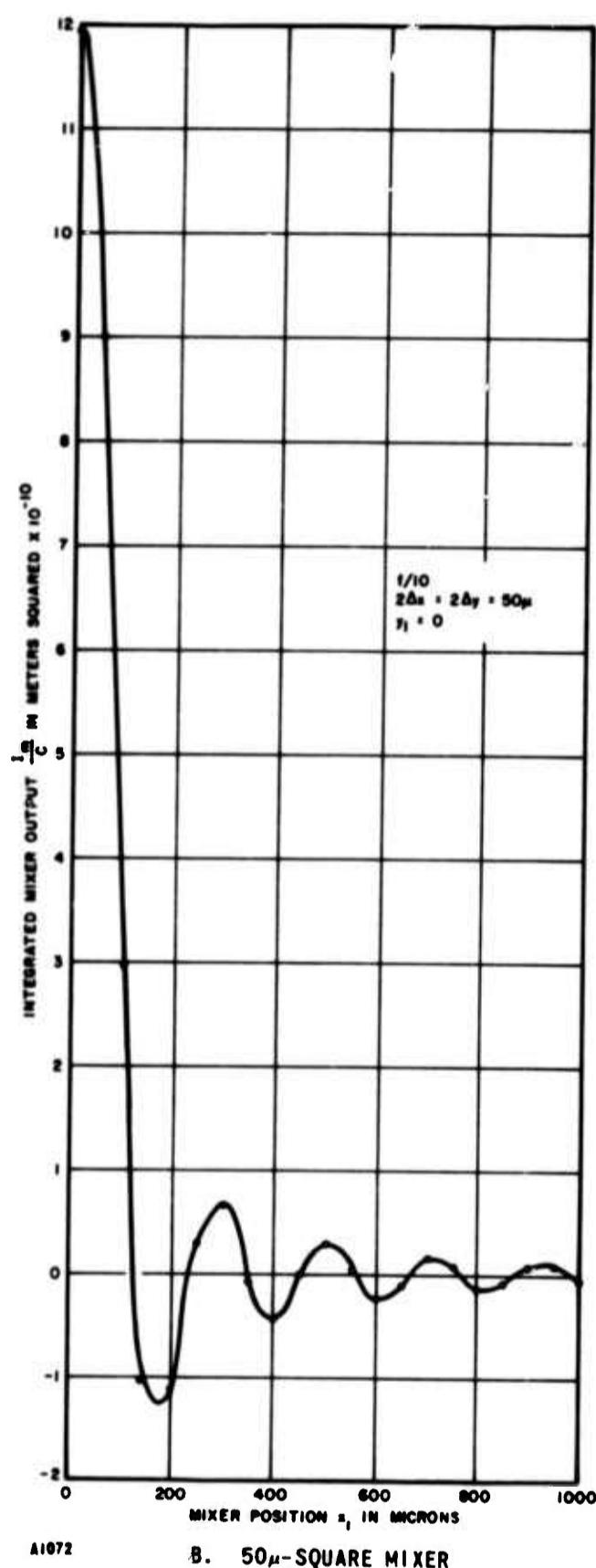
FIGURE 2-2.   CALCULATED HETERODYNE RECEIVER BEAM PATTERN (SHEET 2 OF 5)
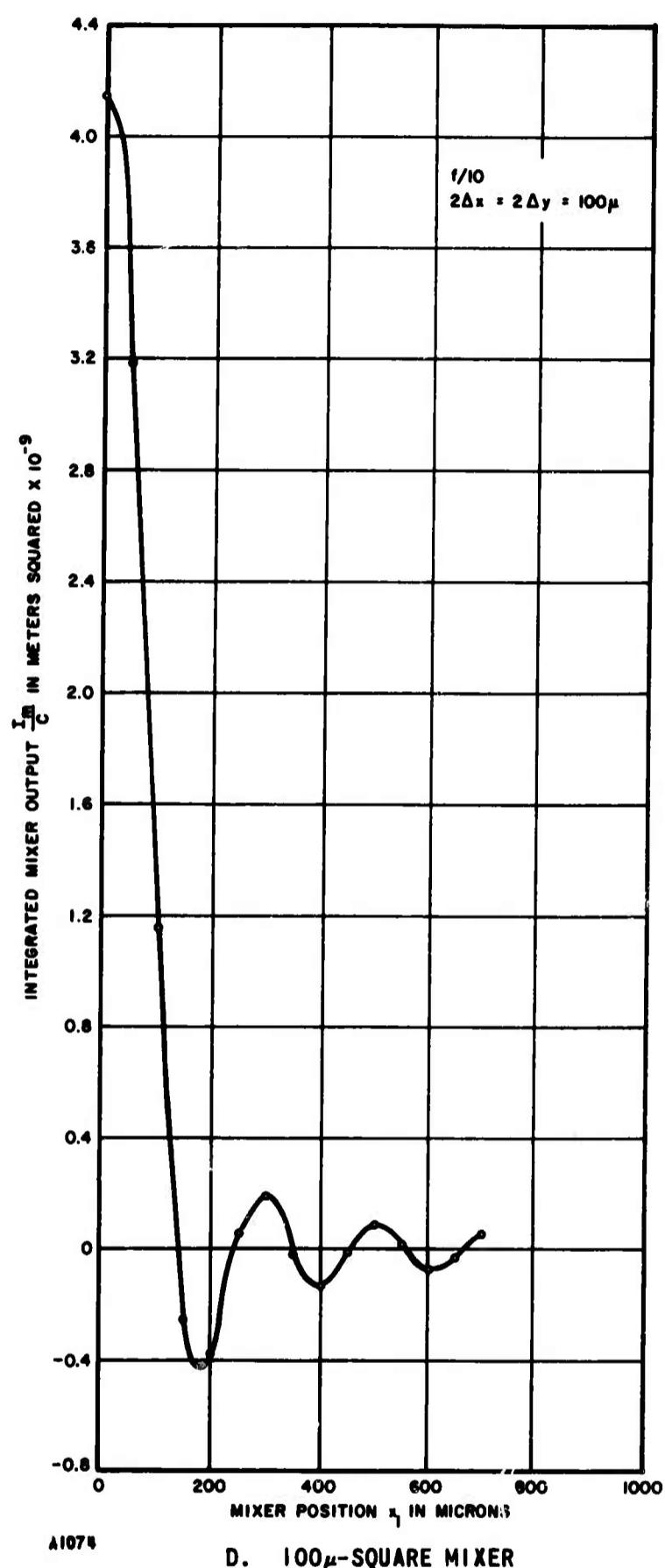
9

Y-axis label: INTEGRATED MIXER OUTPUT $\frac{I_m}{c}$ IN METERS SQUARED X 10^{-9}

Chart annotations:
f/10
$2\Delta x = 2\Delta y = 80\mu$
$y_1 = 0$

X-axis label: MIXER POSITION x_1 IN MICRONS

A1073

C. 80μ-SQUARE MIXER

FIGURE 2-2. CALCULATED HETERODYNE RECEIVER BEAM PATTERN (SHEET 3 OF 5)

FIGURE 2-2. CALCULATED HETERODYNE RECEIVER BEAM PATTERN (SHEET 4 OF 5)

INTEGRATED MIXER OUTPUT $\frac{I_m}{C}$ IN METERS SQUARED $\times 10^{-9}$

VARIABLES

○ $y_1 = 0$, x_1

✕ $x_1 = x_1$, $\left(x_1^2 + y_1^2\right)^{\frac{1}{2}}$

f/10

$2\Delta x = 2\Delta y = 200\mu$

$$\frac{I_m}{C} = \int_{y_1-\Delta y}^{y_1+\Delta y} \int_{x_1-\Delta x}^{x_1+\Delta x} \frac{J_1\left\{\frac{k_0}{f}\left[(x+x')^2 + (y+y')^2\right]^{\frac{1}{2}}\right\}}{\frac{k_0}{f}\left[(x+x')^2 + (y+y')^2\right]^{\frac{1}{2}}}\, dx\, dy$$

HORIZONTAL CUT PATTERN

DIAGONAL CUT PATTERN

MIXER POSITION x_1 IN MICRONS

A1075

E. 200μ-SQUARE MIXER
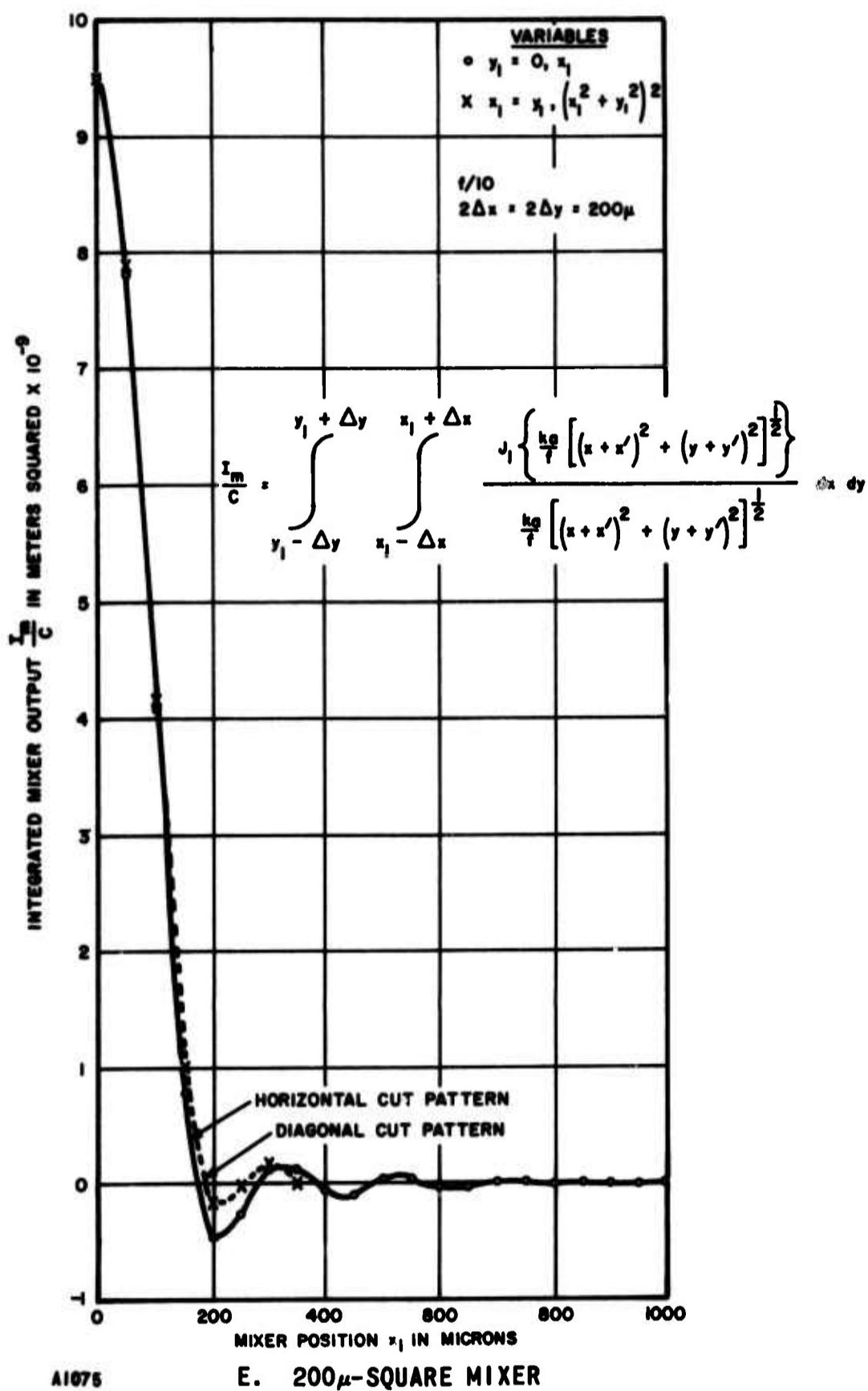
FIGURE 2-2. CALCULATED HETERODYNE RECEIVER BEAM PATTERN (SHEET 5 OF 5)

With this selection of parameters, the diameter of the first dark ring is computed as 258 micrometers. This is seen in Figure 2-2A. This pattern, for a 10 by 10 micrometer mixer, was intended as a probe of the image plane amplitude distribution, as seen by an infinitesimal element. The results compared well with a plot of the function $J_1(x)/x$. For larger mixer areas, the receiving pattern is a combination of the diffraction pattern of the aperture $J_1(x)/x$ and the diffraction pattern of the square mixer $\frac{\sin(x)}{x}$.

In Figures 2-2B, C, D, and E the curves for 50, 80, 100, and 200 micrometer mixers have similar patterns, although the absolute values of the mixer output vary strongly with mixer size. The dotted curve of Figure 2-2E is obtained by sequencing x_1 and y_1, simultaneously, in steps of 35 micrometers each. This gives the pattern along a main diagonal of the array. The main beam is only slightly affected by this diagonal sequencing and there is an inward shift of the side lobes.

When the coordinates of the center of the signal patterns (x', y') are used as the variables in these integral computations, the curves obtained are identical with those obtained in Figure 2-2. Since sequencing (x', y') represents the process of scanning a point target across the field of view, the patterns obtained are also the far-field diffraction patterns of the mixer element.

From this correspondence between the position in the image plane of the receiving aperture and the angle of arrival of the signal radiation, it is apparent that, for a given set of parameters, two receiving beams can be squinted at any angle (within the region of validity of the derived expression) with respect to each other by selecting their relative position in the image plane.

2. SINGLE ELEMENT PATTERN MEASUREMENTS

To verify the computed diffraction patterns and to provide a means for testing actual array responses, a coherent optical pattern measuring range, operative at 10.6 micrometers, was designed, assembled, and put into operation. The antenna range is shown schematically in Figure 2-3 and the laboratory setup is shown in Figure 2-4.
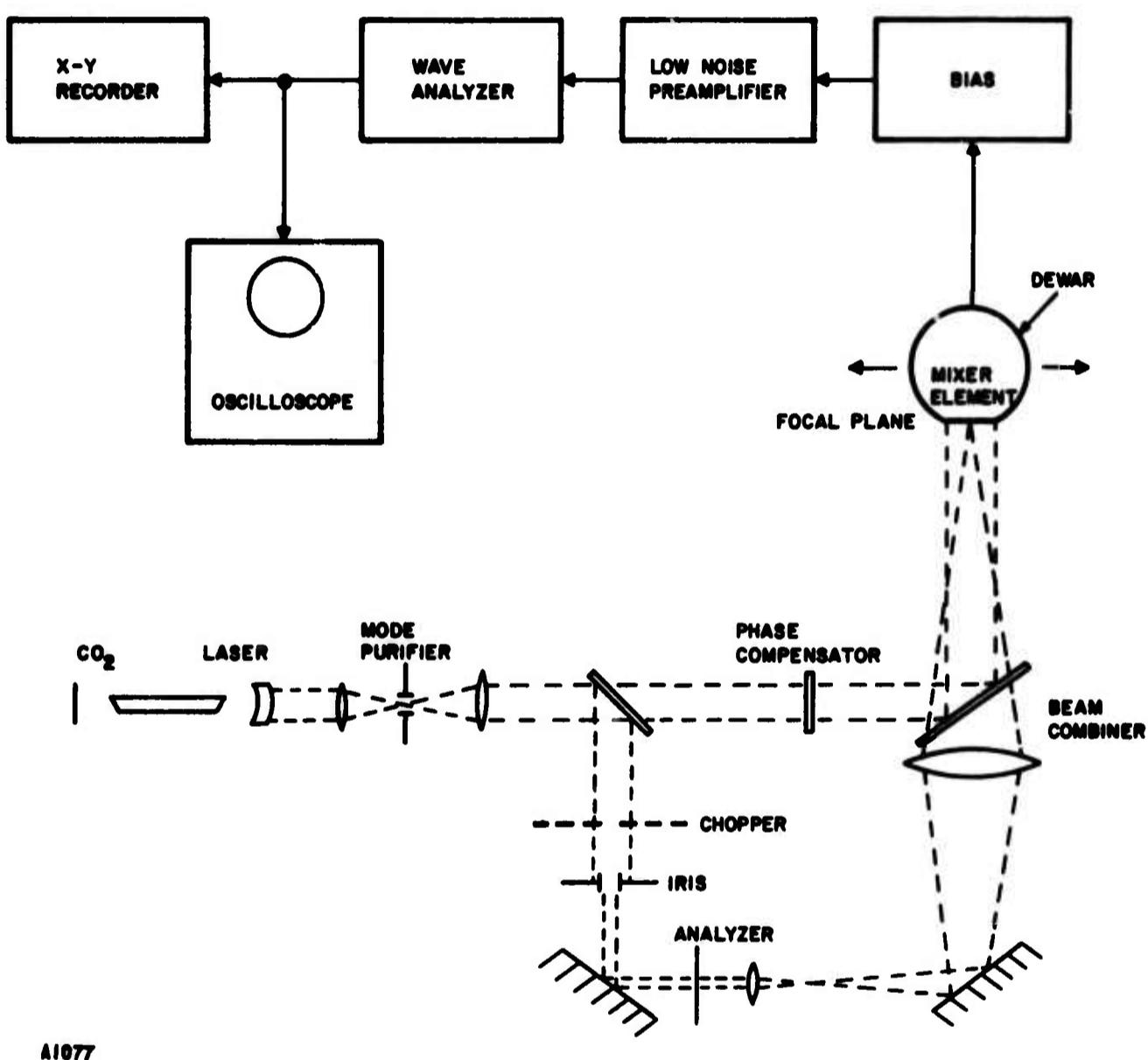
FIGURE 2-3. SCHEMATIC DIAGRAM OF COHERENT OPTICAL ANTENNA PATTERN
MEASURING RANGE

14
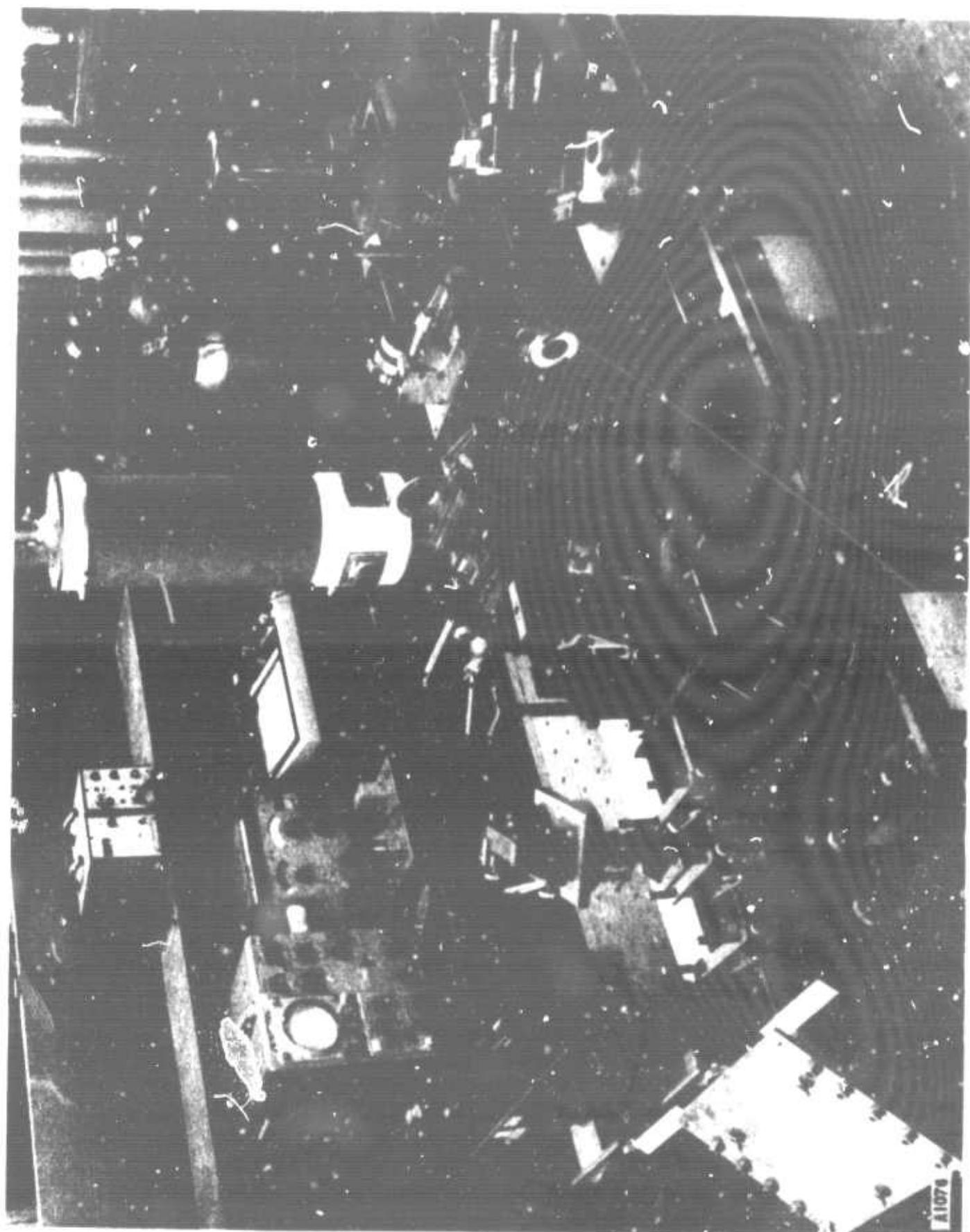
FIGURE 2-4. COHERENT OPTICAL ANTENNA PATTERN MEASURING RANGE OPERATING AT 10.5 MICROMETERS

15

The antenna range is basically a homodyne configuration in which the 10.6-micrometer laser output is split into a local oscillator beam and a signal beam which are individually shaped and then recombined and detected by a mixer element. The mixer (in its dewar) is mounted on vertical and horizontal translation stages. It is motor-driven in the horizontal plane, and tied directly into a X-Y recorder.

A number of diffraction patterns were measured. They are shown as plots of the mixed signal voltage as a function of mixer position in the image plane of the receiving lens. The parameters which were varied in these tests were the f/number of the receiving optics, the detector size, and the diameter of the expanded beam at the receiving aperture.

In one experiment a vertical cut through the focused spot was taken. The measured data is shown in Figure 2-5. A calculated curve for the same parameters is also shown in Figure 2-5 for comparison. The width of the beam at the points where the peak value falls to 50 percent is calculated as 160 micrometers and measured to be 150 micrometers (Figure 2-5), well within experimental error. The width of the first null in the pattern is calculated to be 280 micrometers and measured as 270 micrometers. Similarly, the position of the peak of the second ring and the intensity expected at that point are also in very close agreement; the peaks occur 350 micrometers apart for the calculated curve and 350 micrometers apart for the calculated curve and 350 micrometers apart for the experimental one. Measurements beyond this value were limited by noise in the system. It can be concluded that the measured shape of the image plane pattern (which corresponds to the far-field diffraction pattern) is in very close agreement with the computer predictions.

Horizontal cuts through the focal plane were made, automatically, and plotted on the X-Y recorder, rather than point by point. Figure 2-6 shows a plot of the local oscillator intensity in registration with the field amplitude of the mixed signal.

During preliminary measurements, some interesting results were obtained with the optical antenna pattern measuring range. Figure 2-7 shows automatically measured
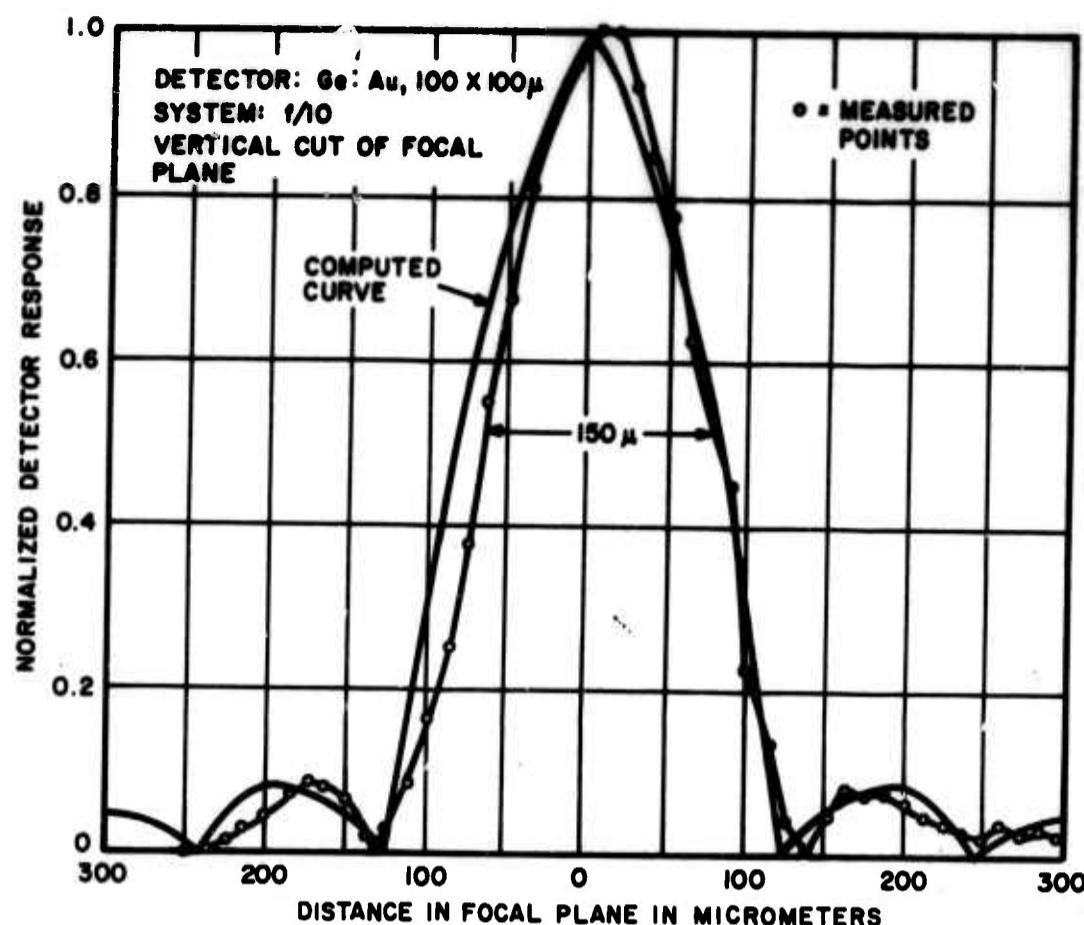
FIGURE 2-5. DATA FOR VERTICAL CUT THROUGH FOCUSED SPOT WITH LOCAL OSCILLATOR

mappings of the IF component of the optical field pattern obtained at several positions relative to the geometrical focus of the receiving aperture. These patterns at 10.6 micrometers are different from the classical intensity patterns. They were taken to give detailed data on the diffraction limited focal volume and to assure that the pattern range was operating satisfactorily.

B.   IMAGE DISSECTOR

In the design of the two-dimensional array, one principal task is the partitioning, or dissection, of the image plane of the receiving aperture into well-defined areas whose signal energy is absorbed by associated mixer elements. A pattern of mixer elements that completely fills the image plane without intervening optics is not feasible because

17
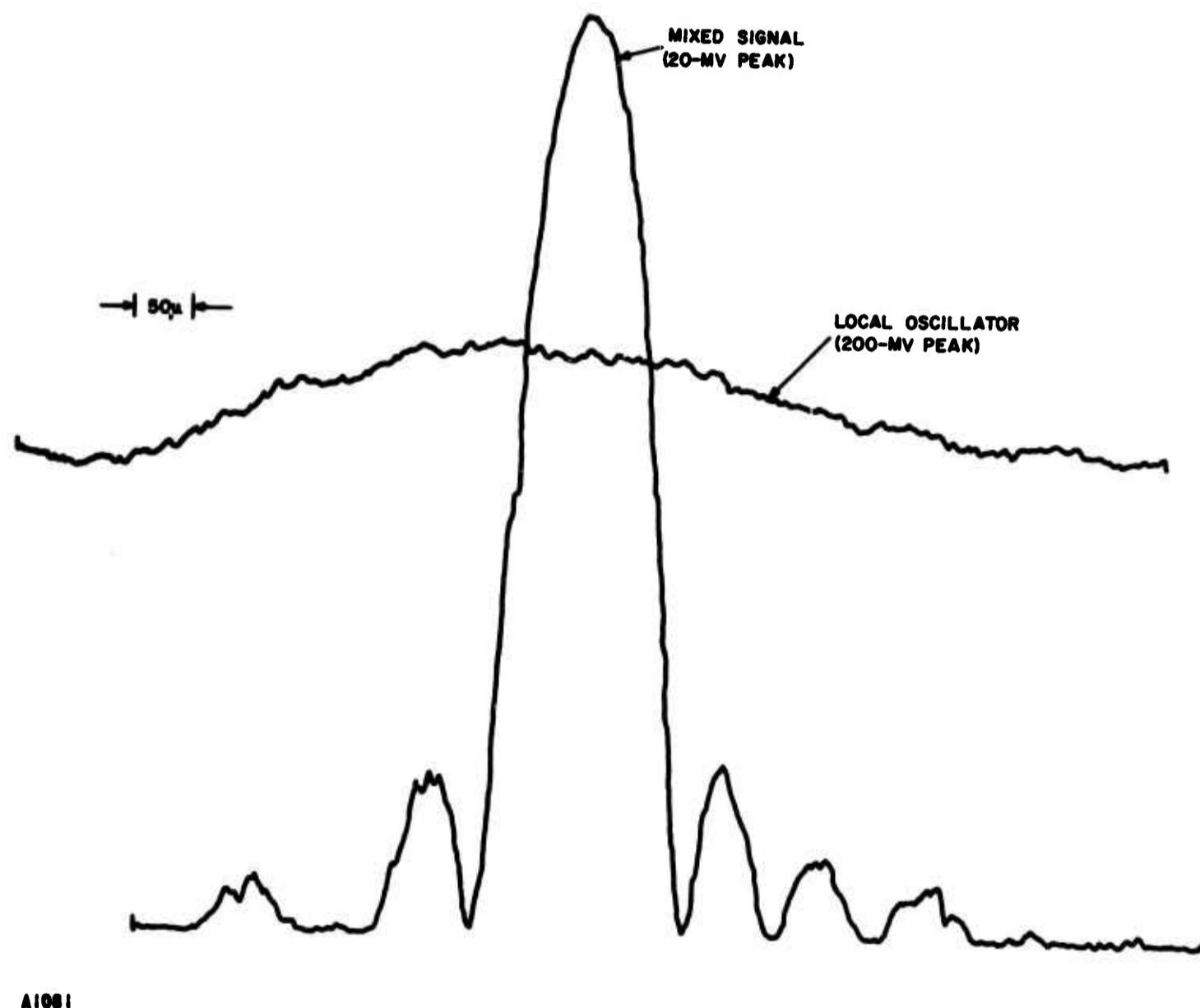
FIGURE 2-6.   MEASURED MIXED SIGNAL FIELD AMPLITUDE AND LOCAL OSCILLATOR
INTENSITY FOR AN f/8 SYSTEM

18

(24)	0.925 INCH	
(23)	0.900 INCH	
(22)	0.875 INCH	
(21)	0.850 INCH	
(20)	0.825 INCH	
(19)	0.800 INCH	
(18)	0.775 INCH	
(17)	0.750 INCH	
(16)	0.725 INCH	
(15)	0.700 INCH	
(14)	0.675 INCH	
(13)	0.650 INCH	
(12)	0.625 INCH	
(11)	0.600 INCH	
(10)	0.575 INCH	
(9)	0.550 INCH	
(8)	0.525 INCH	
(7)	0.500 INCH	
(6)	0.475 INCH	
(5)	0.450 INCH	
(4)	0.424 INCH	
(3)	0.400 INCH	
(2)	0.375 INCH	
(1)	0.350 INCH	90μ
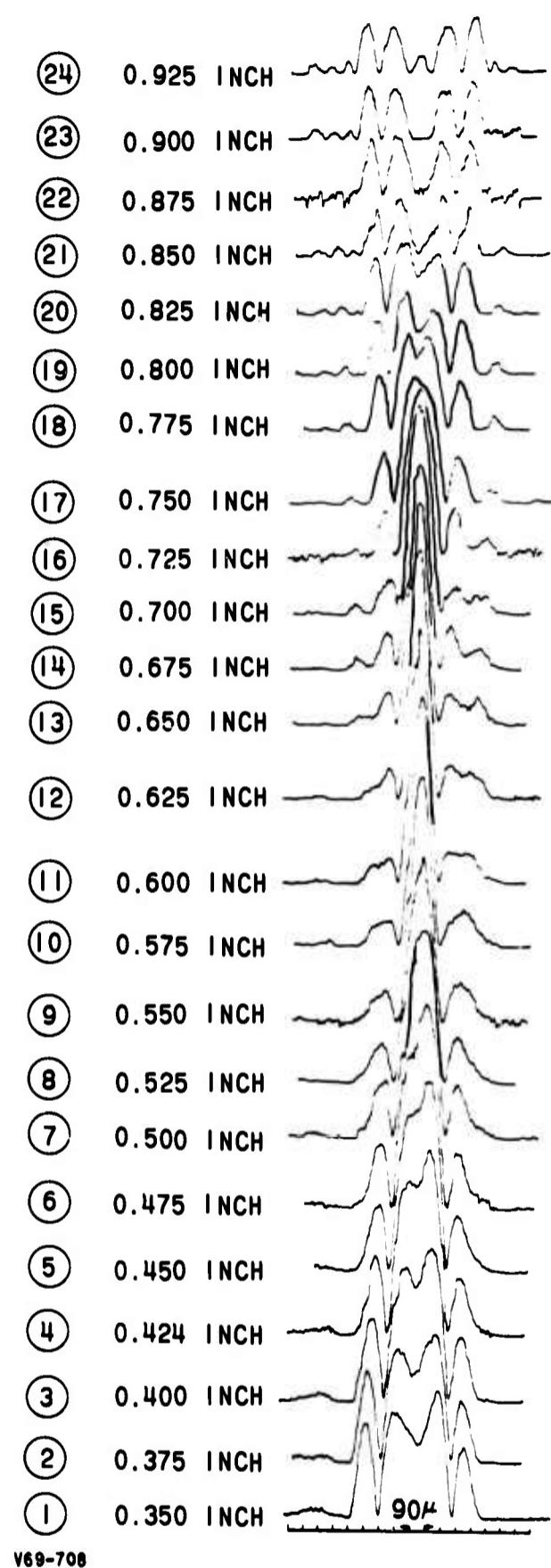
V69-708

FIGURE 2-7. AUTOMATICALLY MEASURED MAPPINGS OF FIELD AMPLITUDE (IF COMPONENT)

separation is required between elements for cabling, cooling, and electrical shielding. However, space between elements, when not properly matched by optics, represents receiver inefficiency. For example, a spacing between elements equal to the element width involves a loss of 75 percent of the available signal energy. Since detailed consideration of the required spacing leads to significantly greater spacing than one element in width, the inefficiency of not matching the mixer area to the image plane area becomes prohibitive. For this reason, optical elements are required to match each subdivision of the image plane to the smaller mixer element assigned to it.

Several alternative approaches were considered for dissecting the image plane. Two of these were brought to the hardware phase; namely a refracting multifaceted device and an array of microlenses.

A beam of electromagnetic energy traversing a multifaceted high refractive-index material will be dissected by the discontinuities at the facet edges and its segments dispersed into a divergent pattern. By this technique the partitioned areas in the image phase are separated from one another to permit using relatively isolated mixer elements. The mixer elements are placed where the partitioned areas are sufficiently separated but within the depth of focus of the image volume. The device of Figure 2-8 was designed for this task and some cursory tests were performed with it. This approach was considered to be of limited use because it is not readily extended to larger arrays than 3 ×3 and there is no flexibility in the dissected image size for matching to the small mixer element assigned to it.

The array of microlenses consists of an arrangement of small thick lenses that fill the image phase and dissect it into subdivisions that are reduced in area by a factor of 25 to match the capture area of each mixer element of the receiving array. Figure 2-9 shows the microlens structure with only three lens installed to show some details.

20
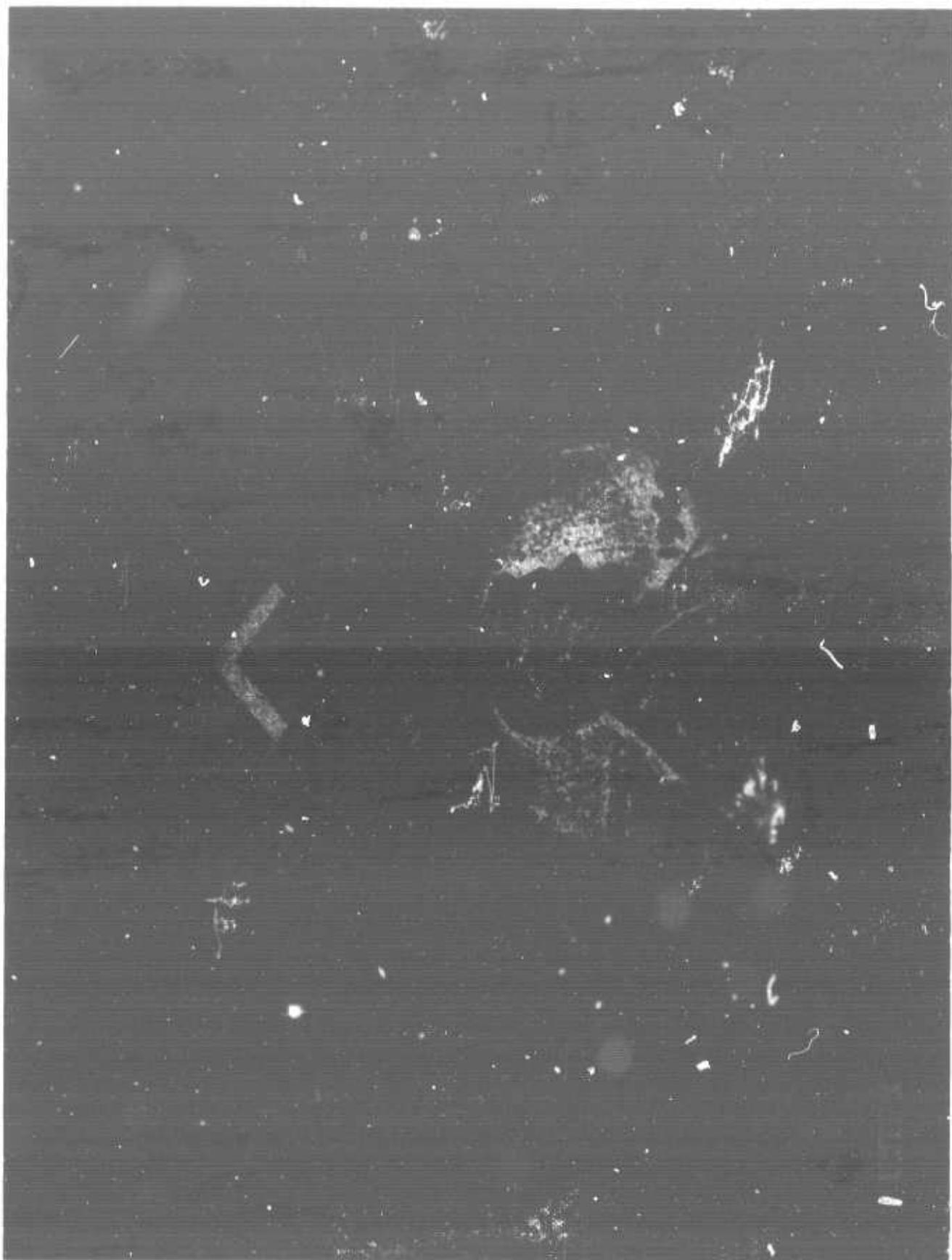
FIGURE 2-8. REFRACTING IMAGE DISSECTOR
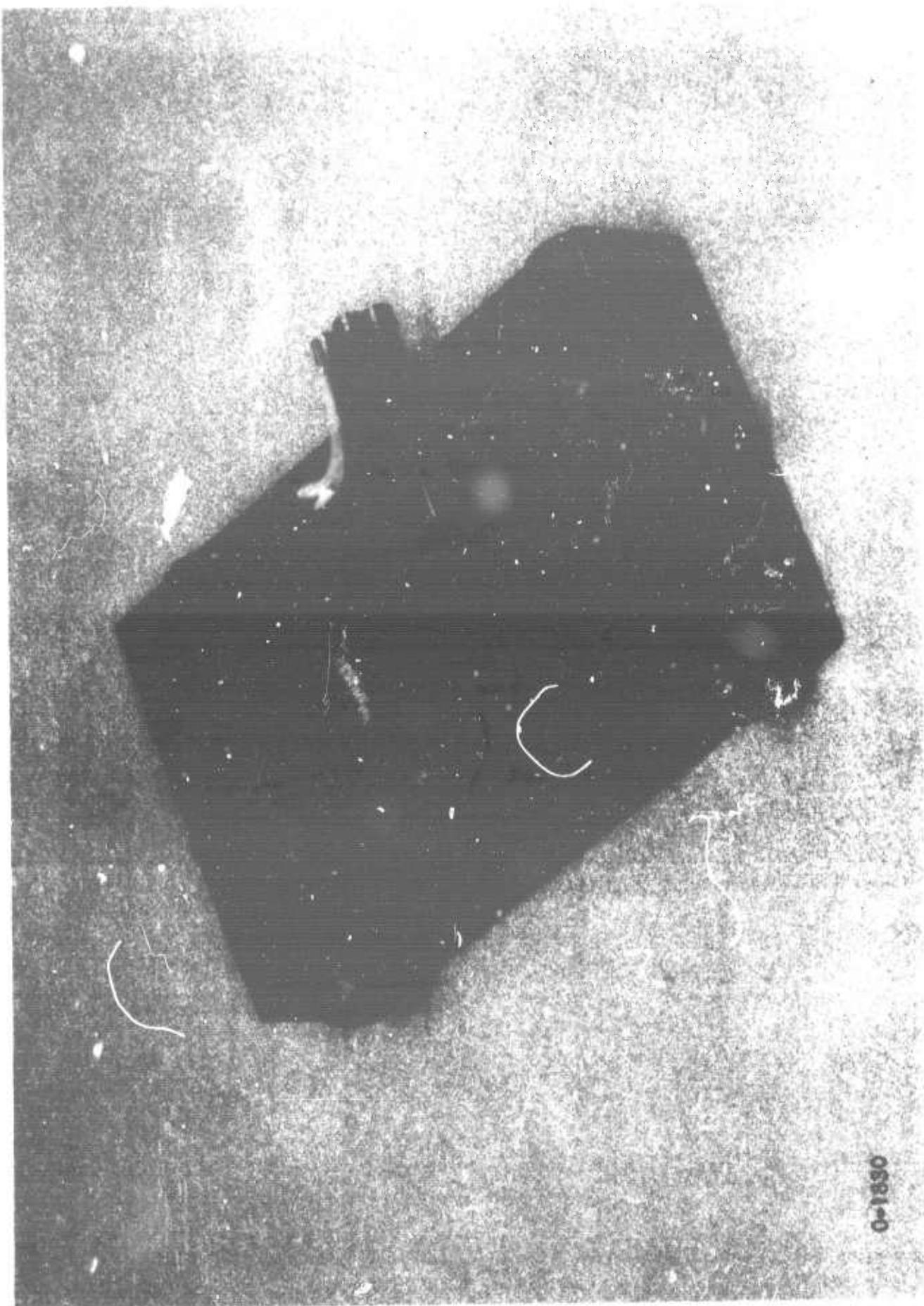
FIGURE 2-9. MICROLENS IMAGE DISSECTOR

O-1830

In the next set of measurements the test configuration was arranged so that a large focused diffraction-limited spot of low level input combined with a phase wave from the local oscillator is incident on the 3 × 3 array of microlenses. The array dissects the combined signals into nine components that are spatially matched in size and position to the 3 × 3 array of mixer elements in the focal plane of the microlenses. For the first of these measurements the input spot was produced by an optical system with nominally f/100* speed at 10.6 micrometers. The low-level signal was chopped at a 20 Hz rate, combined with the laser plane wave, and spatially scanned by a small mixer element (100 × 100 micrometers). The IF component (20 Hz) of the mixer output was selected by a narrowband tuned amplifier and automatically recorded as Figure 2-10A. This is a plot of the field amplitude (not the intensity) of the IF component of the total field at the input to the array of microlenses. The shape, relative size, and relative position of the main lobe and its side lobes indicate a reasonable approximation to the $J_1(x)/x$ form predicted by the analysis (Section II. A. 1).

The microlenses, whose relative size is indicated in the figure, each take a portion of the diffraction-limited spot and the local oscillator wave and reduce it to match the wideband mixer elements in the array. In one measurement the large spot was centered on the middle microlens and the output focal plane of the array was scanned and recorded as before. The output IF components of the total field are shown in Figure 2-10B. The noteworthy characteristic of this output is its relatively clean noiseless appearance with little phase or amplitude perturbation. There were no edge effects or generation of higher order modes. In practice a mixer element would be spatially matched to each of these output spots to maximize the optical mixing efficiency of the array.

The next series, Figure 2-11 are successive plots taken as the input spot is incrementally scanned across the array, simulating a change in angle of arrival of the

_____

* A later calibration showed this to be actually f/93.

A. DIFFRACTION-LIMITED INPUT TO MICROLENS ARRAY

B. MICROLENS ARRAY OUTPUT
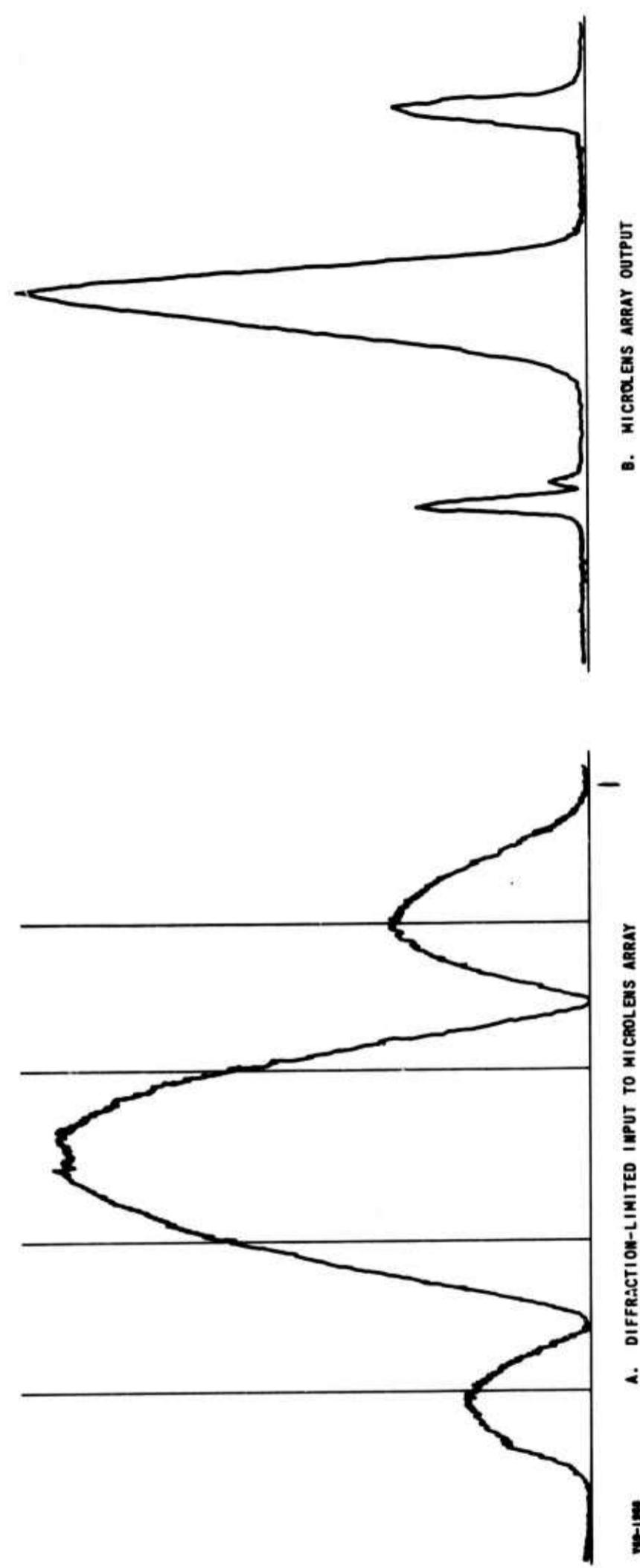
FIGURE 2-10. PLOT OF MICROLENS PATTERNS
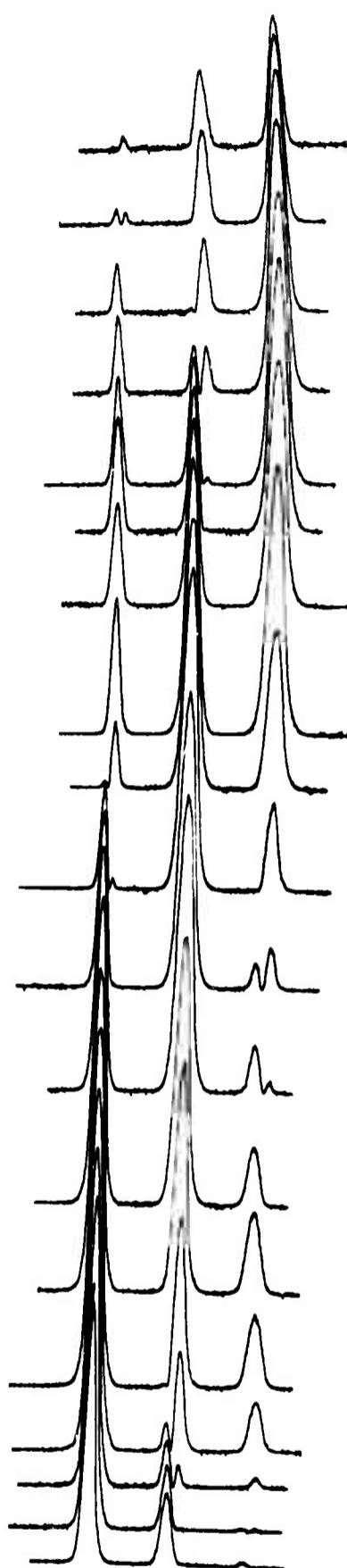
V69-1602

FIGURE 2-11. SUCCESSIVE PLOTS WITH INPUT SPOT INCREMENTALLY SCANNED

small-signal radiation. The rise and fall of the optical side lobes are clearly shown. The double peak at some positions results when the null in the input pattern falls exactly on a microlens. Since a 180 degree optical phase reversal is associated with this null the mixer output also produces a null when the IF energies associated with each phase are equal and cancel.

In the next measurement each mixer was held fixed in the focal plane of its associated microlens and the input spot was scanned across the array by sweeping the input angle of arrival through a small angle. These data were recorded point by point for three array elements and are shown in Figure 2-12. Each pattern represents a far field "receiving antenna" pattern for the associated optics and mixer element. The abscissa represents position in the focal plane and is linearly related (for small angles) to the angle of arrival of the incoming signal. Together these patterns characterize a multilobe multielement receiving system with squinted beams (the classical amplitude sensing monopulse receiver at microwaves uses a 2 × 2 array of such beams). The crossover points for adjacent beams are determined by the f/number of the optics, the wavelength, and the center to center spacing of the microlenses (see the analysis in the first semiannual report, reference 1). In this case the lenses were designed to give 3-dB crossovers for an f/100 spot at 10.6 micrometers. Since the actual spot was found to be f/93 the crossovers would be expected to occur further down from the peak than the 3-dB design values. When compared to the values at the central peak, the left crossover is 4.0 dB and the right one is 3.7 dB. For f/93 and 1.1 millimeter center to center spacing for the lenses the computed crossover value is 3.6 dB. This number agrees closely with the measured values and further validates the analytical model selected to guide the development of this array.

In Figure 2-12 differences may be seen in the peak values obtained for the three patterns. These are due to small variations in the system parameters for each

26
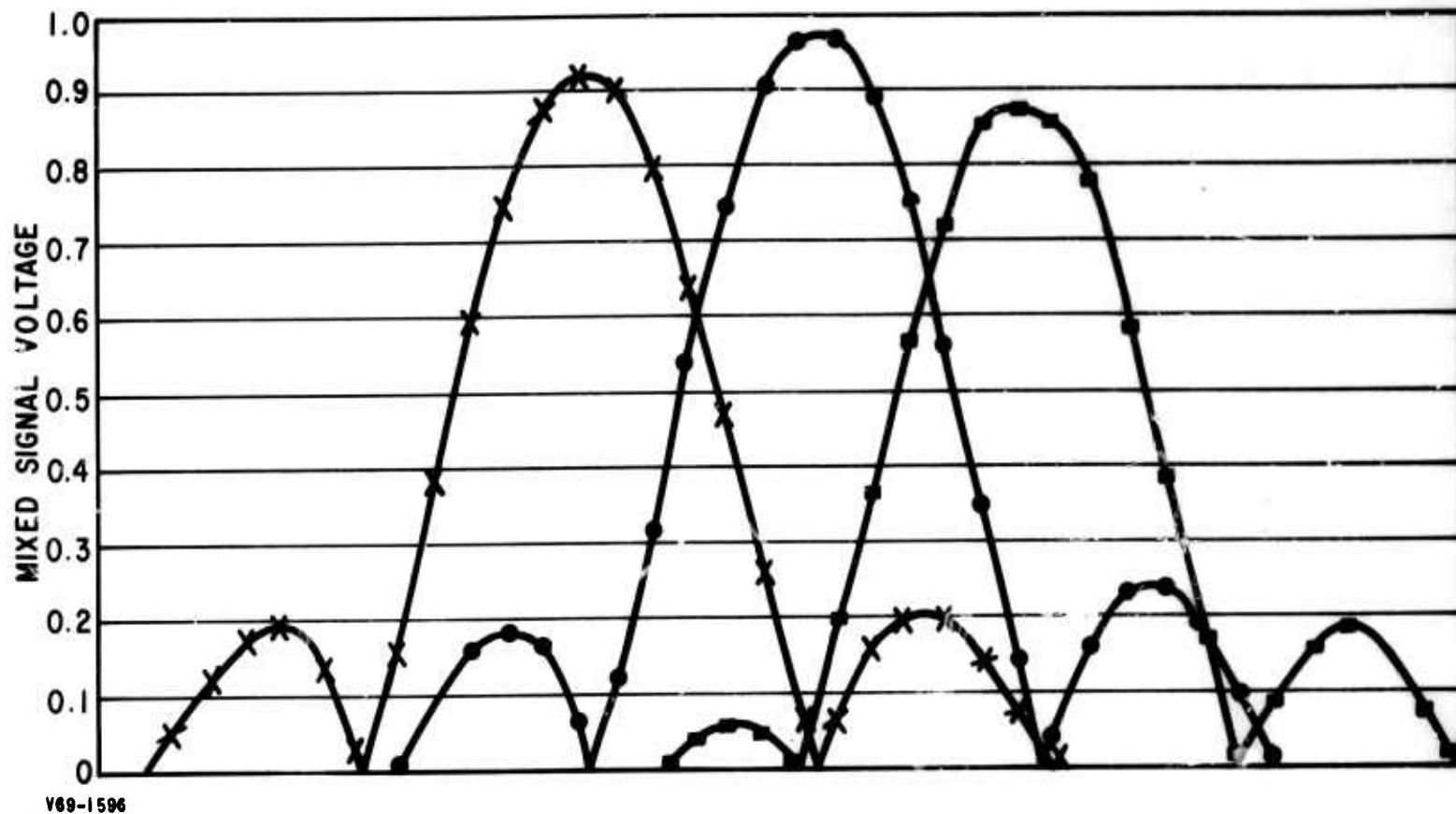
FIGURE 2-12. RECEIVING PATTERNS FOR THREE MICROLENSES IN REGISTRATION

position in the array. In practice these variations could be compensated by individually adjusting the dc bias currents to each mixer element and possibly the channel amplifier gain settings.

No mention has as yet been made of the level of the optical side lobes and possible problems that might arise from them in a system application. For purposes of developing this array, analytical and laboratory models that used the $J_1(x)/x$ field pattern for the IF signal component were adequate and useful. However, if in a practical system it should become desirable to reduce the side lobes or reshape the main beam, classical microwave or optical techniques such as illumination taper (apodization) may be employed here.

C.   ARRAY STRUCTURE

The mixer elements for use in this application have a square cross section and are several times longer than they are wide to obtain the necessary quantum efficiency. A structure was needed that would support this kind of element and provide sufficient thermal conducting material for adequate cooling at 4.2 K, low-loss transmission lines for use up to 1.5 GHz, and electrical isolation to minimize crosstalk between elements. The structure of Figure 2-13 was designed to meet these requirements. It consists of copper plates with inserts of microwave microstrip. A mixer element is mounted in each of the slots and connected to a 50-ohm microstrip transmission line matched into a coaxial connector.

A thermal analysis of the copper structure for 3×3 elements shows that for the highest values of bias and local oscillator power to be expected in operation the central mixer element would undergo a temperature rise of less than 1 K when operating in a liquid helium dewar. This temperature rise is well within design tolerances, so that the structure design was judged to be satisfactory. Should this design have to be extended to 10×10 or more elements a more elaborate analysis would be required. However, there seems to be sufficient design margin available in the maximum dissipation per element, the maximum permissable temperature rise, and the material used in the structure.

D.   MICROSTRIP

Two approaches were considered for cabling the microwave IF signal from the mixer to the preamplifiers; microcable and microstrip. The microcables were very small thin-walled coaxial cables with outside diameters from 0.008 to 0.020 inches. After experimentation with short samples of these cables the problem areas were found to be supporting them, connecting to them at both ends, and the poor shielding predicted for the thin outer walls. In comparison these problems for the microstrip case had been solved on other AIL programs and the technology was applicable here. The microstrip cabling was selected.

28
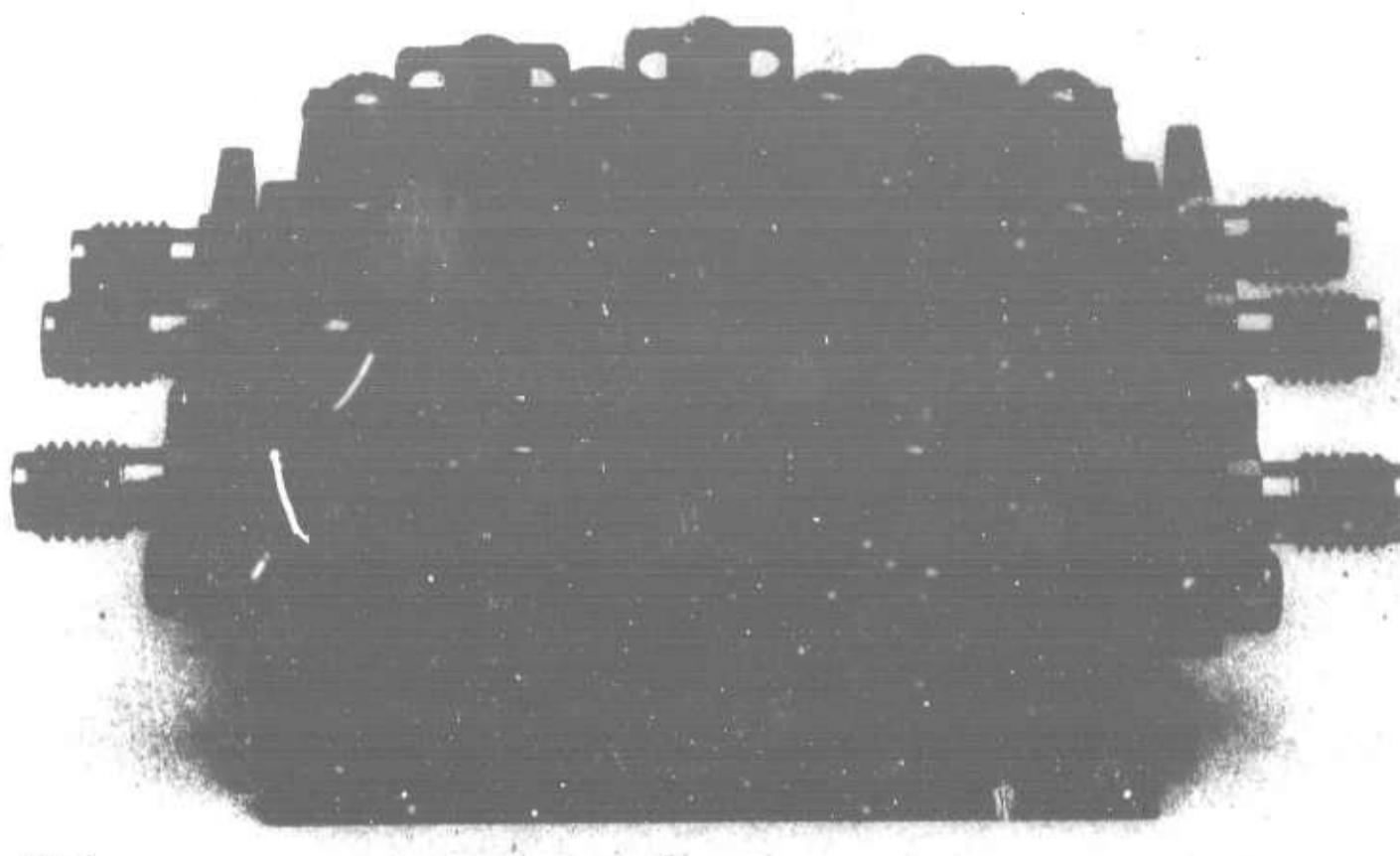
FIGURE 2-13. ARRAY STRUCTURE

The microstrip design consists of thin films of conducting material deposited onto alumina substrates. One side is completely covered with conducting material to provide a ground plane. The other side has deposited conducting strips as shown in Figure 2-14. This unit is then placed into a recess in the copper plate and connections made to it at the mixer elements and at the connectors.
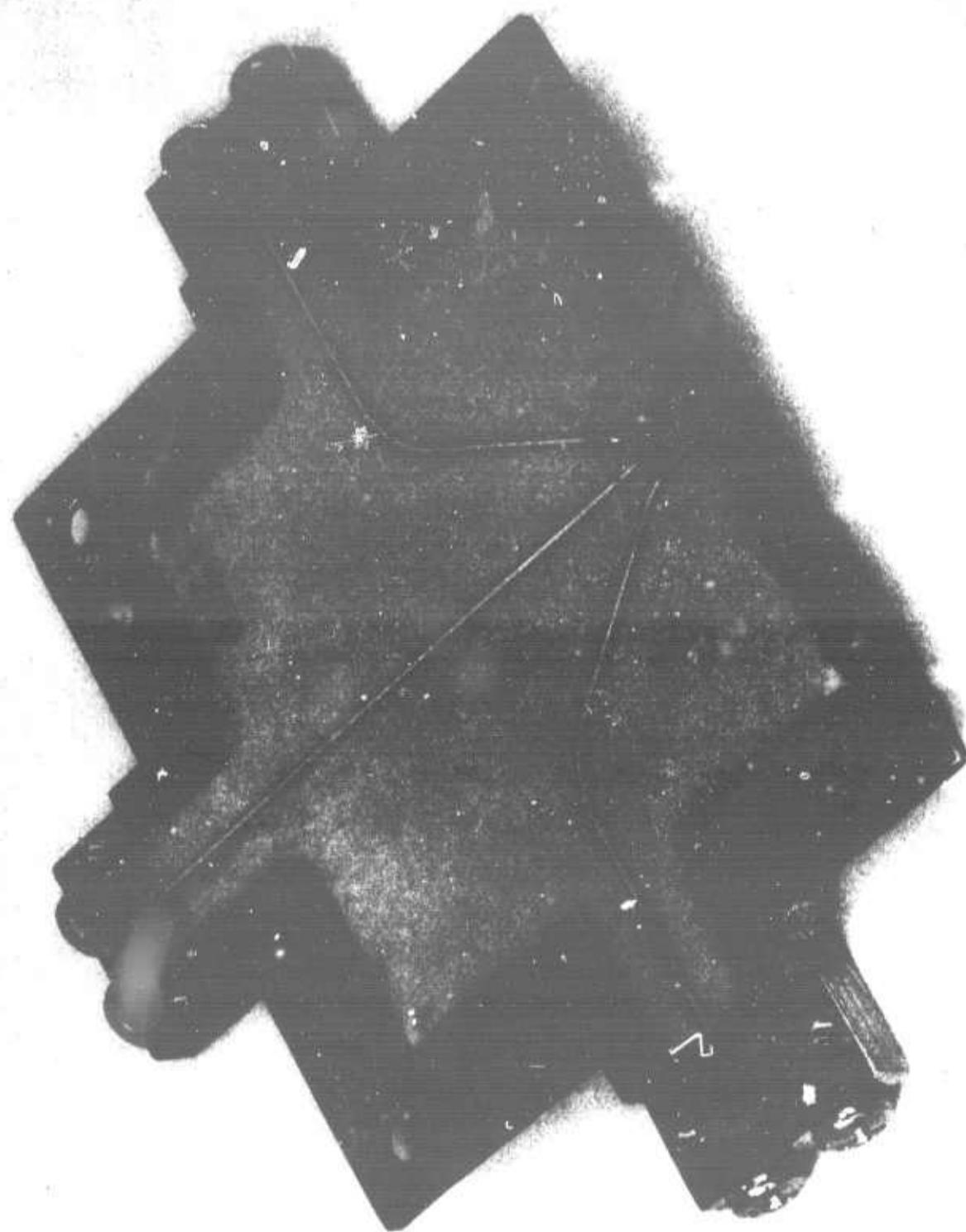
FIGURE 2-14. MICROSTRIP CABLING

0-1831

III. 1.5-GHz MIXER DEVELOPMENT

A. APPROACH

The design of the 10.6-micrometer mixer for this program is governed by the following objectives:

- High sensitivity, with operation near the quantum-noise limit

- Large instantaneous frequency response (10 MHz to 1.5 GHz)

- Low-noise, wideband IF amplifier optimally coupled with the mixer

- Minimum power dissipation required for local oscillator and dc bias (to achieve required performance)

- Highest possible operating temperature

In this section, experimental data toward the above objectives (on photoconductive mixers and analyses on photovoltaic 10.6-micrometer mixing) are presented.

B. PHOTOCONDUCTIVE MIXERS

A program recently completed at AIL (under NASA sponsorship) obtained explicit engineering equations useful in the design of optimum infrared receivers. These engineering equations involved such parameters as: local oscillator power, dc bias power, IF amplifier noise temperature, mixer-IF interface, mixer resistance, and mixer material parameters. The results of this analysis, with specific application to gigahertz bandwidth 10.6-micrometer high-sensitivity receiver development, have been published (reference 2).

In the approach that was developed, infrared mixer performance was expressed in terms of two principal factors:

- Noise attributable to the mixer element itself

- IF amplifier noise referred to the mixer input through the conversion gain term, which quantitatively describes the ability of the frequency-translation process to convert the available infrared signal to IF signal

Examination of the expressions for conversion gain and noise equivalent power provide the following criteria for quantum-noise-limited large-IF-bandwidth infrared mixer design:

- High mixer quantum efficiency

- Carrier lifetimes in the subnanosecond region

- Low mixer resistance, achieved by sufficient laser local oscillator power

- Short carrier transit times in the mixer

- Low mixer capacitance

- Linear mixer operation, including absence of carrier depletion due to excessive local oscillator power

- Low-noise IF amplifier

Only a few infrared detector materials are candidates for meeting the above criteria. These materials include Ge:Cu, Ge:Hg, Si:Al, HgCdTe and PbSn (Te, Se). Photoconductive Ge:Cu, in which compensation significantly decreases carrier lifetime, is a prime candidate. This material is useful for heterodyne operation from approximately 5 to 30 micrometers.

Measurements on compensated Ge:Cu, as a mixer material, were given in reference 2 and its successful application in a packaged unit is described in references 3 and 4.

C.   SELECTION OF PHOTOCONDUCTIVE MIXER MATERIAL

The development of a 1.5-GHz mixer-preamplifier combination for the present program was based on: (1) extending the technology developed for a single-channel 10.6-micrometer 1-GHz heterodyne receiver, and (2) examining other mixer materials.

While there are a number of interrelated parameters, the frequency response of a PC mixer element is largely limited by the carrier lifetime, τ. Figure 3-1 shows the variation of conversion gain (G) with IF frequency for three values of τ. Two ordinates are shown, depending on what value is taken for transit time. Note that a variation in G with

32
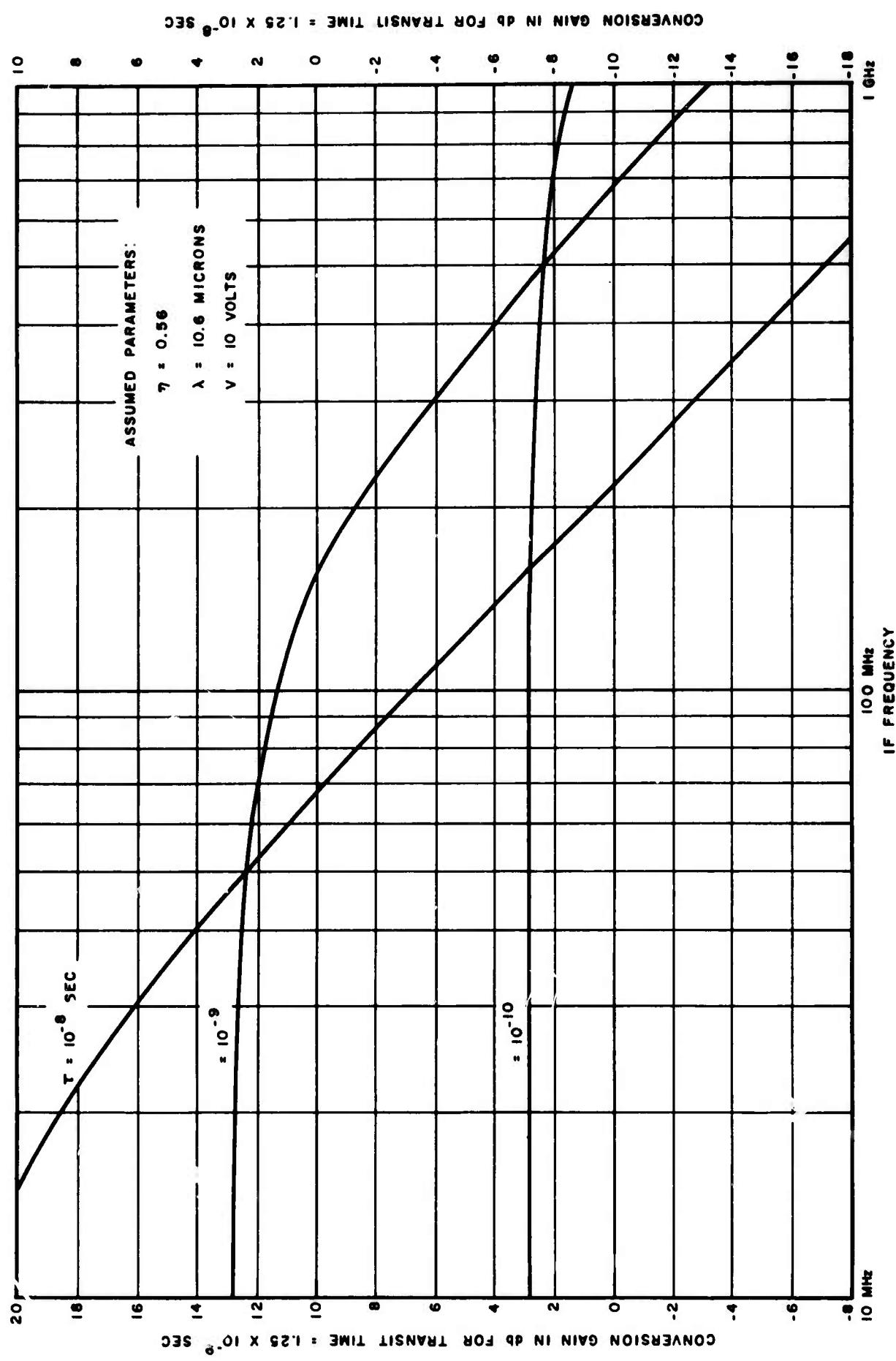
FIGURE 3-1. CALCULATED VARIATION OF CONVERSION GAIN WITH FREQUENCY FOR THREE VALUES OF LIFETIME

33

IF frequency does not necessarily indicate that receiver sensitivity will vary in the same manner; what matters for quantum-noise-limited performance is the frequency range over which the conversion gain is sufficient to override IF amplifier noise. A gain-equalizing network may be used in the IF where receiver sensitivity has already been established.

Whereas frequency response increases with decreasing carrier lifetime, the available mixer gain increases with τ, resulting in a gain-bandwidth constraint. Figure 3-1 shows that in order to extend frequency response to 1.5 GHz, and beyond, it is desirable to reduce τ in order to increase G at the higher frequencies. This has the effect of decreasing G at the lower frequencies, but this is not necessarily a disadvantage since the IF noise factor is usually lower at the lower frequencies. The decrease in τ is accomplished by increasing the impurity-doping in the mixer element.

Since many of the design considerations are interrelated, the final choice of mixer material for the array is determined by experimentation based on the analytical considerations mentioned above.

The following sections present test data on nine mixers (five Ge:Cu, one Ge:Hg, one Si:Al, and two HgCdTe). The measurements were carried out using a low-noise broadband IF amplifier whose characteristics are described further in Section III-G.

D. COPPER-DOPED GERMANIUM

Copper-doped germanium photoconductive detectors offered the most promise for this application. Overall receiver sensitivity can be optimized by minimizing the ratio of the effective IF input noise temperature to the available conversion gain. Extensive noise measurements were made as a function of IF frequency, dc bias, and local oscillator power, to determine the mixer-preamplifier combination offering the best combination of sensitivity, frequency response, and power dissipation.

34

A Ge:Cu mixer element (No. C-1) similar to the one used in the packaged receiver (reference 3) as well as one with higher (No. C-2) and one with lower (No. C-3) compensation levels were tested up to the 1.5-GHz region.

1. Ge:Cu NO. C-1

The previously-measured available G-R noise (quantum noise referred to mixer output) power, as a function of frequency of mixer element C-1 is shown in Figure 3-2 for two values of dc bias power. The method of measurement was described in reference 2. By a substitution technique, the G-R noise output from the mixer element alone is measured directly under operational conditions, with laser local oscillator power applied. This measurement yields the values for τ and μ, since

$$\overline{I_{GR}^2} = \frac{4q\tau\mu B}{L^2 \left(1 + \omega^2 \tau^2\right)} \, P_{dc}$$

where

$\overline{I_{GR}^2}$ = mean-square G-R noise current,

P_{dc} = dc bias power

The experimentally-measured G-R noise power rolls off at about 6 dB/octave as the above equation predicts, with the 3-dB roll-over frequency at approximately 750 MHz, yielding $\tau = 2 \times 10^{-10}$ sec. This 3-dB point is called the mixer roll-over frequency, f_{c-m}.

Measurements were made on mixer C-1 integrated with an early-model wideband IF amplifier (Figure 3-3). The methods used give an indirect measurement of receiver (mixer-preamplifier combination) sensitivity as a function of frequency. It is performed by measuring the total noise (G-R noise and thermal noise) relative to thermal noise only, and referring the ratio to an absolute measurement of NEP under low-frequency quantum-noise-limited conditions. The receiver roll-over frequency, f_{c-r}, is defined as the frequency

35
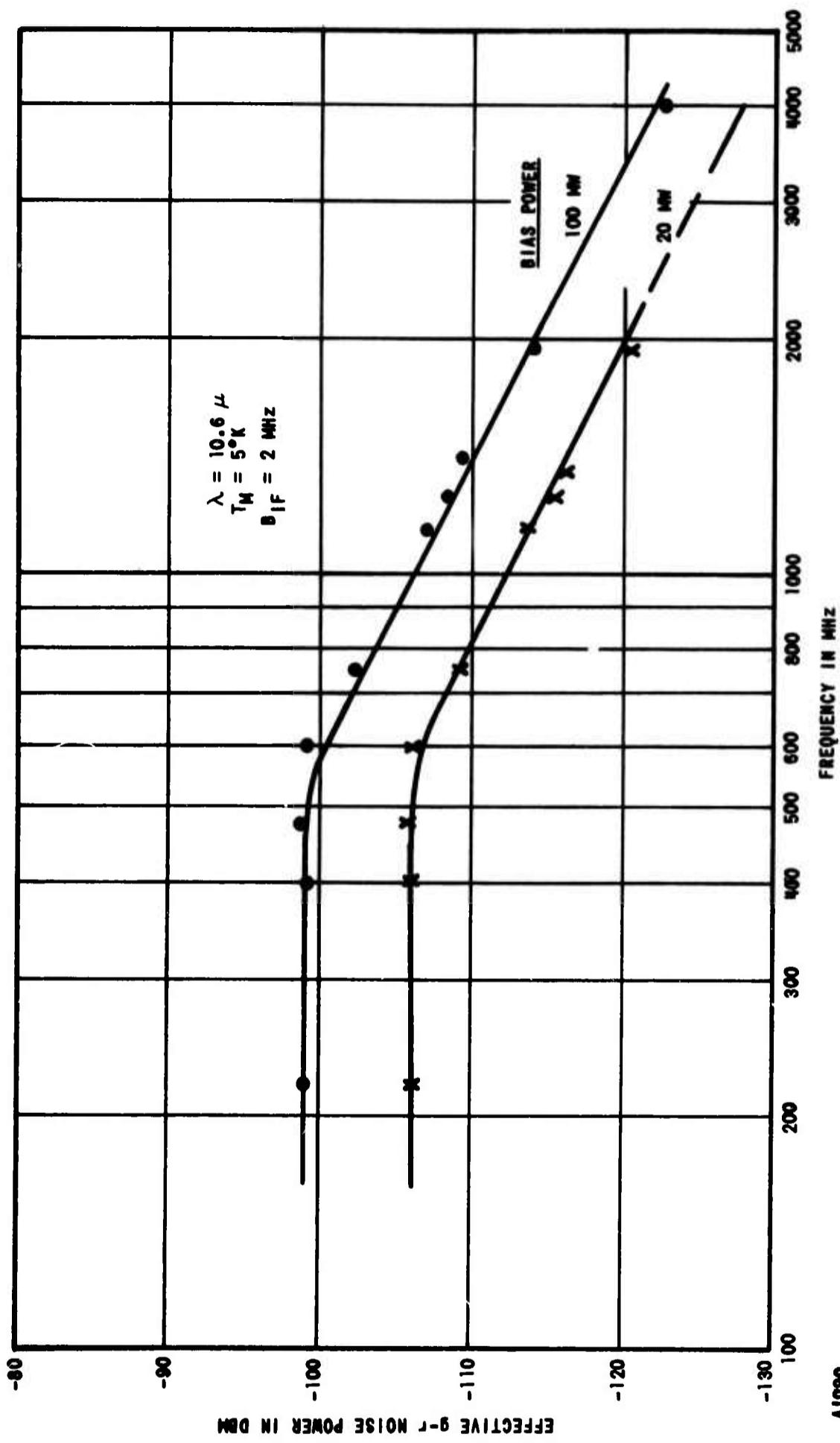
FIGURE 3-2. MEASURED G-R NOISE POWER FOR MIXER NO. C-1
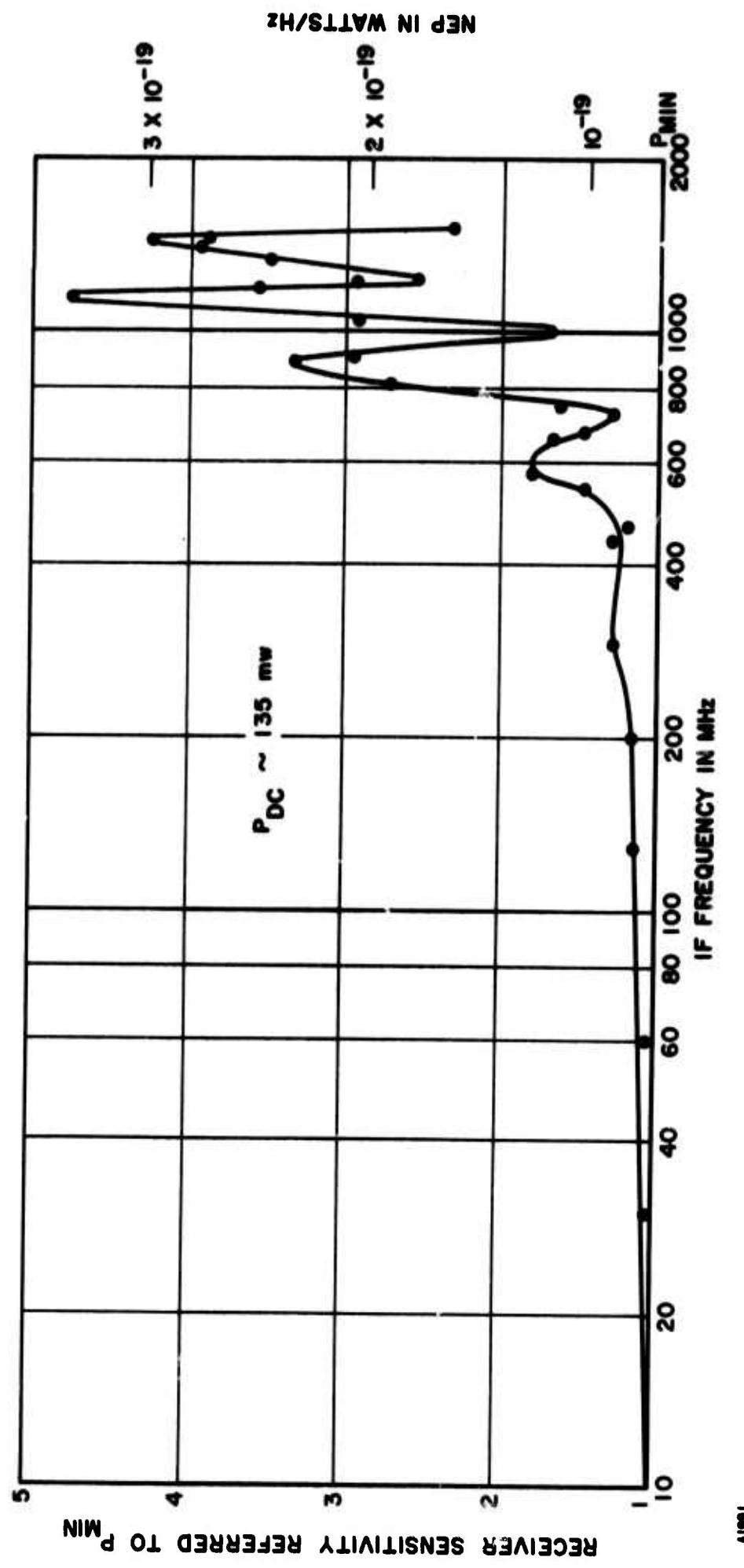
FIGURE 3-3. RECEIVER SENSITIVITY VS IF FREQUENCY FOR Ge:Cu NO. C-1

where this ratio first achieves the value 2. The reference value, NEP (hereafter called P_{MIN}) was measured to be 7.5×10^{-20} watt/Hz at an IF of 10 kHz. The dc bias power was 135 milliwatts, and the mixer resistance had been reduced to 1000 ohms by the laser local oscillator. These conditions were maintained throughout the frequency run, up to 1.5 GHz.

The results are plotted in Figure 3-2 on both an absolute scale (watt/Hz) and a relative scale indicating the degradation in performance with frequency. The NEP is less than 1.3×10^{-19} watt/Hz from 15 to 800 MHz, less than 2.4×10^{-19} watt/Hz up to 1 GHz and less than 3.6×10^{-19} watt/Hz up to 1.5 GHz. The peaks and valleys in the performance (with this early-model amplifier and matching network) are due to nonoptimum high-frequency impedance transformations.

Figure 3-4 shows another noise ratio measurement with mixer C-1, using the improved low-noise amplifier discussed in Section III-G. A substantial sensitivity improvement is evident compared to Figure 3-3. The maximum NEP's inferred from Figure 3-3 are 1.5×10^{-19} and 2.7×10^{-19} watt/Hz (from 10 MHz up to 1.43 GHz) for bias voltages of 15 and 10 volts, respectively, and sufficient LO power to reduce mixer resistance to 2000 ohms. The bias voltages correspond to bias power of 112 and 50 milliwatts, respectively.

The measured conversion gain at 10 kHz was approximately +8 and +10.5 dB for the 10- and 15-volt bias conditions.

Receiver roll-over frequencies (f_{c-r}) of 1.43 GHz and 980 MHz were obtained for 15 and 10 volts bias, respectively.

Figure 3-5 shows the I-V characteristics of mixer C-1, with various levels of LO power. The mixer resistance is seen to vary from 150,000 ohms to 400 ohms as the applied LO power is increased. Also note the linearity of the curves, since much of the photoconductive mixer analysis is simplified by this assumption.

38
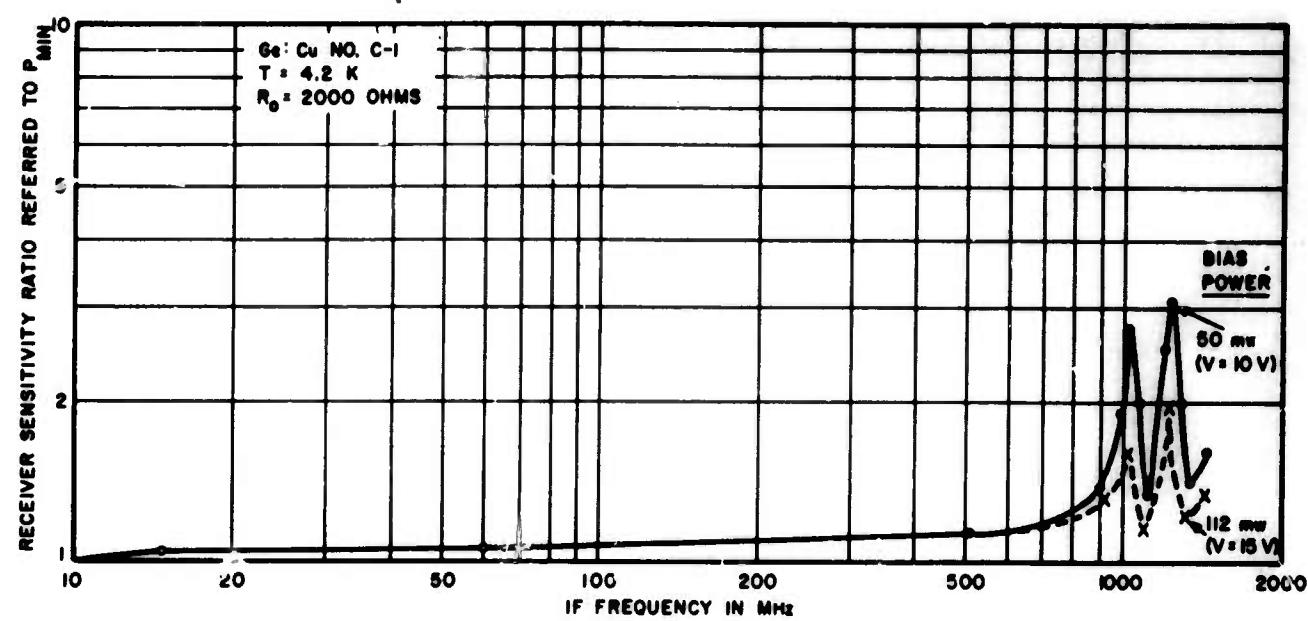
FIGURE 3-4. RECEIVER SENSITIVITY VS IF FREQUENCY FOR Ge:Cu NO. C-1 USING IMPROVED IF AMPLIFIER
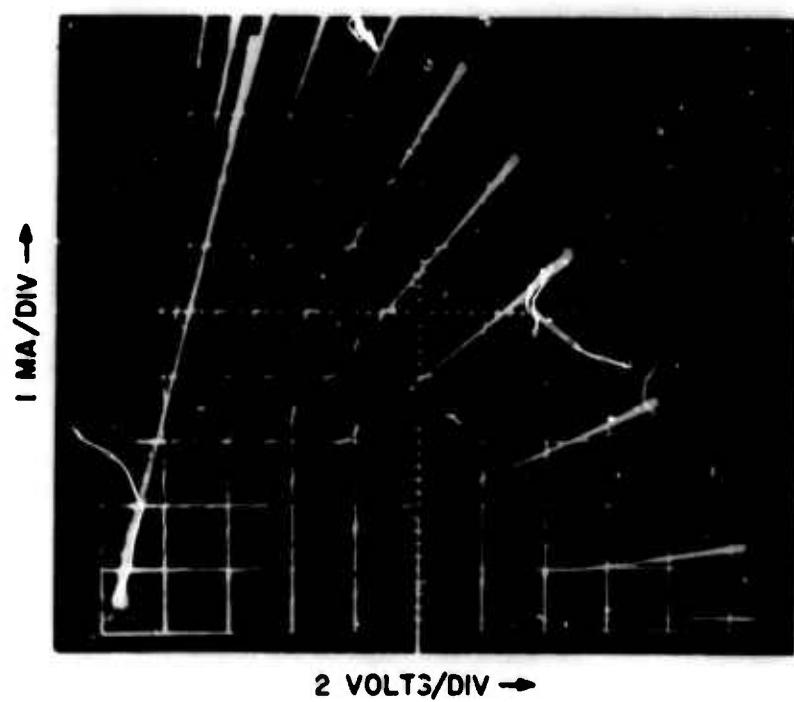
A1093

FIGURE 3-5. I-V CHARACTERISTIC OF Ge:Cu NO. C-1 FOR VARIOUS LASER LO POWER LEVELS

2.   Ge:Cu NO. C-2

Figure 3-6 shows a noise-ratio sensitivity measurement on mixer element C-2, using sufficient LO power to reduce the mixer resistance to 2200 ohms and applied dc bias of 10 and 15 volts. Mixer element C-2 has a carrier lifetime that is estimated to be one-half that of mixer C-1. This was expected to reduce to one-half the available mixer gain at low IF frequencies, and to roughly double the mixer roll-over frequency to the 1.5-GHz region. As can be seen from Figure 3-5, the receiver roll-over frequencies measured were 910 MHz (15 volts applied) and 880 MHz (10 volts applied). These correspond to NEP's of 2.25×10^{-19} and 3.75×10^{-19} watt/Hz respectively.

Comparison of Figures 3-4 and 3-6 shows that mixer C-2 yields poorer performance than mixer C-1, at an IF near 1.4 GHz, for nearly equal mixer resistance and dc bias power values. It was concluded that a mixer element similar to type C-1 will better meet the requirements for the proposed 1.5 GHz array.
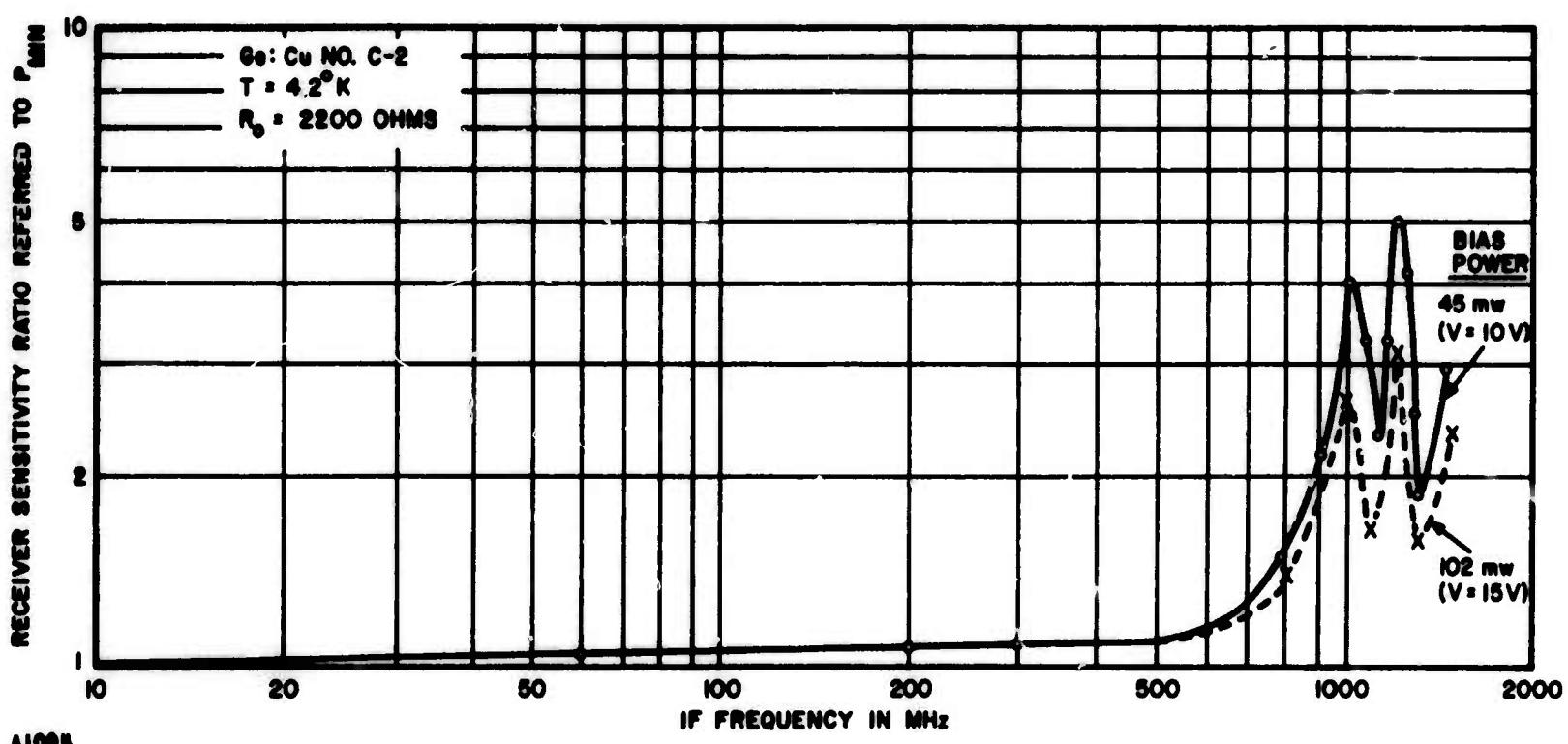
FIGURE 3-6.   RECEIVER SENSITIVITY VS IF FREQUENCY FOR Ge:Cu NO. C-2 USING IMPROVED IF AMPLIFIER

At higher IF frequencies, up to 2 GHz, the C-2 mixer element should provide better receiver noise performance. Preliminary measurements of mixer C-2 with a laboratory low-noise IF amplifier (1- to 2-GHz passband) resulted in indirectly measured noise-ratio sensitivities of less than 7×10^{-19} watt/Hz (up to 1.8 GHz), and less than 12.6×10^{-19} watt/Hz (up to 2.0 GHz) for a mixer resistance of 3600 ohms, and applied bias of 15 volts. These results could be improved by reducing the mixer impedance (by increasing LO power) and improving the nonoptimum IF amplifier.

3. Ge:Cu NO. C-3

The directly measured G-R noise power output of element C-3 is shown in Figure 3-7. This shows that the mixer roll-over frequency is below 400 MHz, as expected.

Noise-ratio sensitivity measurements on mixer element C-3 resulted in poor performance near 1.5 GHz, so that no further measurements were taken.

E. MERCURY-DOPED GERMANIUM

Sensitivity and frequency response measurements were made on a partially-compensated mercury-doped germanium mixer element cooled to 4.2 K. The Ge:Hg element is useful from approximately 9 to 13 micrometers. The indirectly measured noise-ratio sensitivity as a function of IF frequency is shown in Figure 3-8 for an applied LO power sufficient to reduce mixer resistance to 3000 ohms, and a bias voltage of 15 volts. It was concluded, from the degraded low-frequency sensitivity and the low receiver roll-over frequency, that this mixer element is not suitable for a 1.5-GHz receiver.

F. ALUMINUM-DOPED SILICON

Sensitivity and frequency response measurements were made on one aluminum-doped silicon detector element previously investigated by Soref (reference 5). The element had an estimated $\tau = 5 \times 10^{-10}$ s (according to Soref). This value was deemed to be low enough to be of possible use to this program. The indirectly-measured noise-ratio sensitivity, as a function of IF frequency, is shown in Figure 3-9 for an applied LO power
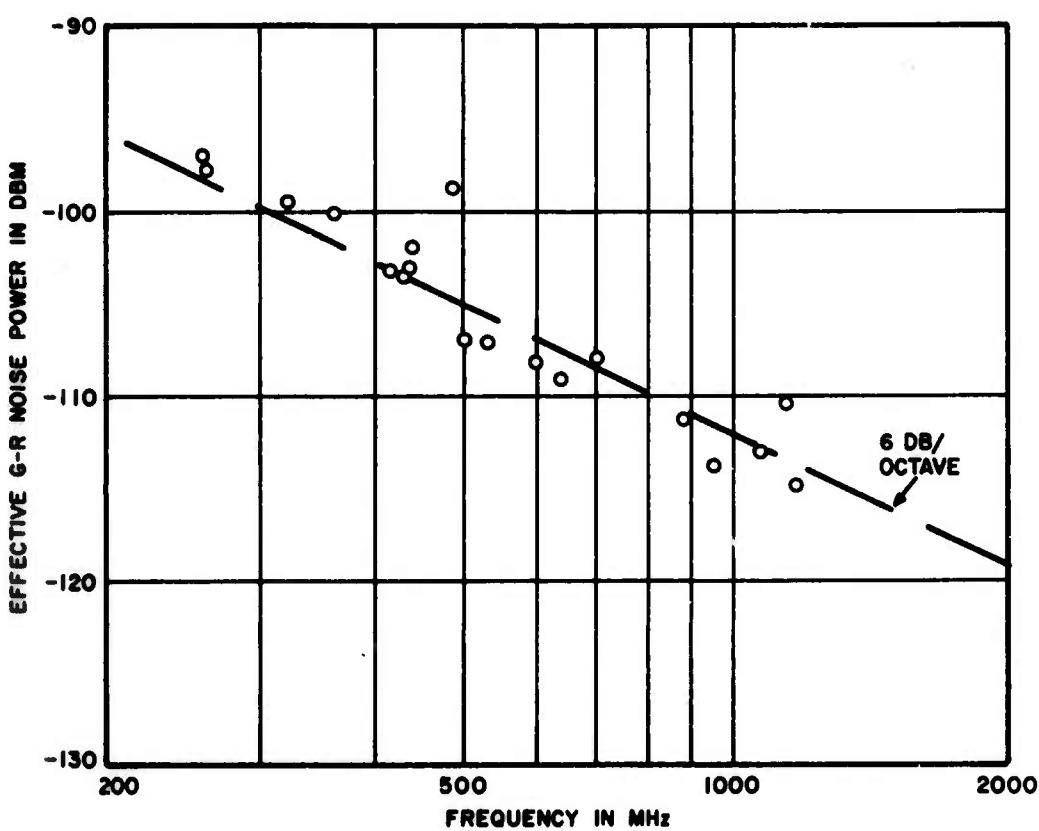
A1095

FIGURE 3-7.   MEASURED G-R NOISE POWER VS IF FREQUENCY FOR Ge:Cu NO. C-3
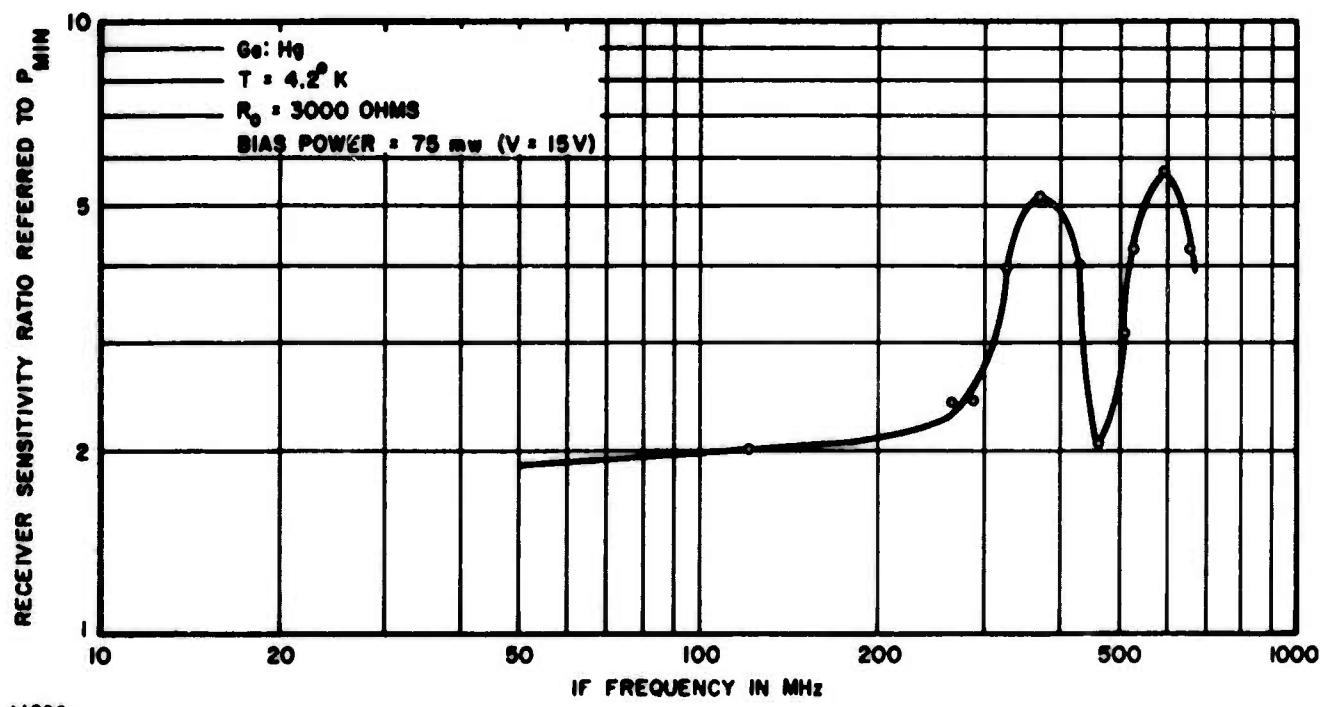
A1096

FIGURE 3-8.   RECEIVER SENSITIVITY FOR Ge:Hg MIXER

42
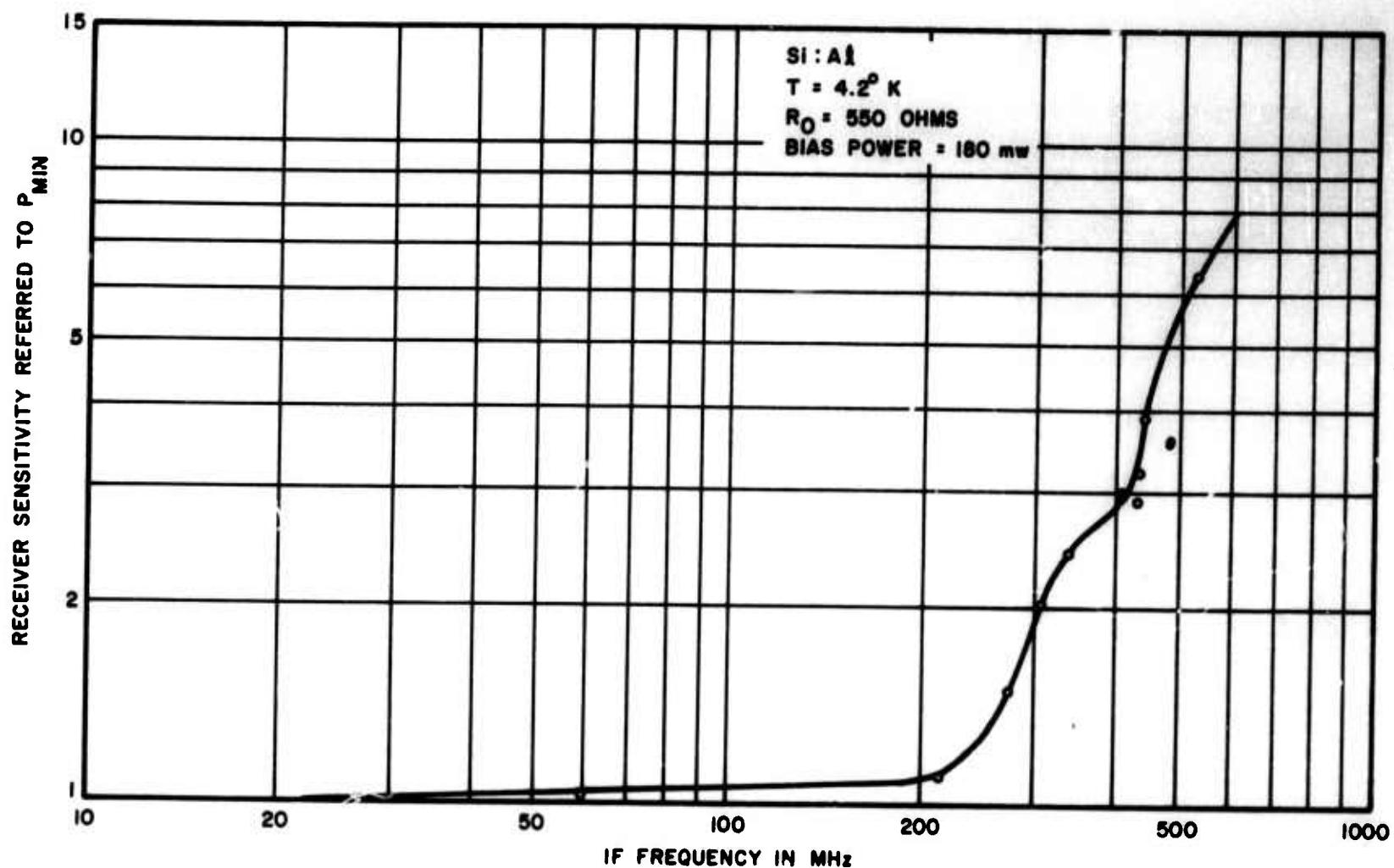
FIGURE 3-9. RECEIVER SENSITIVITY FOR Si:A1 MIXER

sufficient to reduce the mixer resistance to 550 ohms, and a dc bias voltage of 10 volts. The receiver roll-over frequency occurs at approximately 325 MHz. It was not established whether this relatively low value is due to a long carrier lifetime or the large interelectrode capacitance of the nonoptimum element geometry. In any event, this element was not deemed suitable for 1.5-GHz operation.

G.   MERCURY-CADMIUM TELLURIDE

Photoconductive (PC) and photovoltaic (PV) HgCdTe mixer elements were investigated to determine their potential usefulness on this program. Analysis of PC mixer operation has been previously reported (reference 2). A comparable analysis of a PV mixer

has been carried out and is given in detail in Appendix B. This analysis considered conversion gain, NEP, and IF bandwidth in terms of engineering parameters such as diode capacitance, series resistance, shunt conductance, and LO power. (The use of double- and triple-tuned circuits to extend the high-frequency response is also considered.) The analysis uses the same conversion gain approach successfully used in the PC mixer analysis. To date, subnanosecond response times have not been reported for HgCdTe detectors.

Figure 3-10 shows the measured G-R noise output power, as a function of dc bias power, of an experimental photoconductive HgCdTe mixer element, cooled to 77 K. The measurement technique is essentially similar to the one previously used to evaluate germanium detectors. As predicted by the photoconductive analysis, the G-R noise power is directly proportional to bias power and drops off at the higher frequencies.
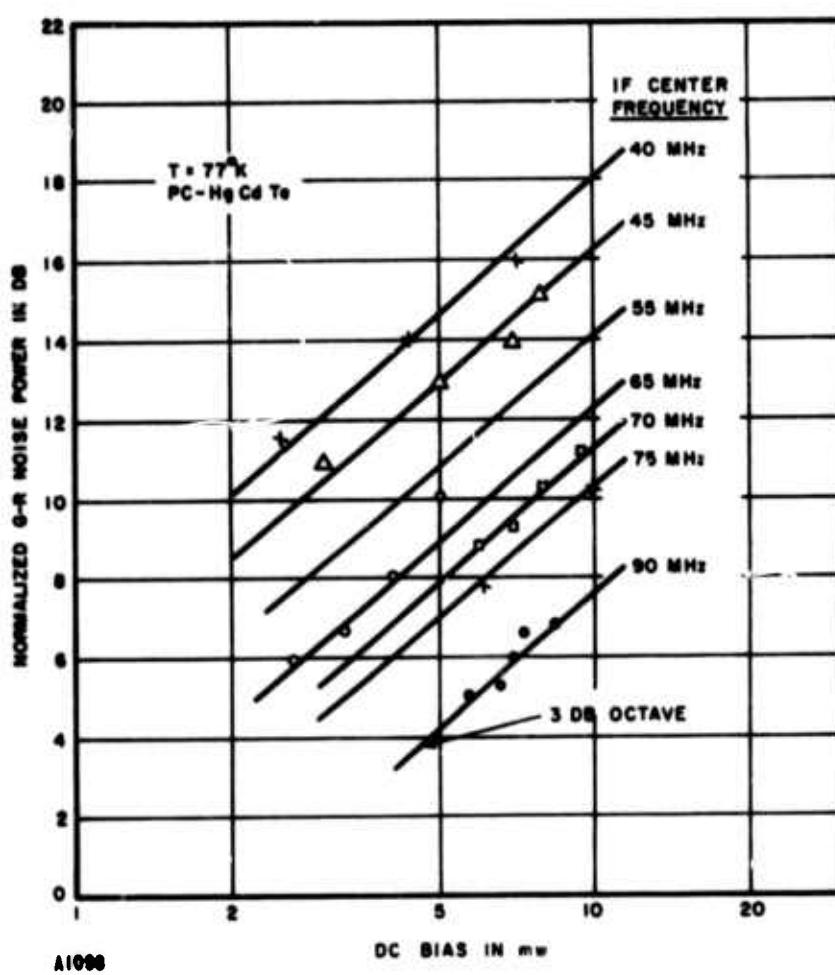
FIGURE 3-10. MEASURED G-R NOISE AS A FUNCTION OF BIAS POWER FOR HgCdTe MIXER

44

Figure 3-11 gives the measured G-R noise power, as a function of IF frequency. The mixer roll-off frequency was too low to be accurately determined with the measurement technique that was employed, and hence is of no interest for the 1.5-GHz application. Preliminary tests on other HgCdTe mixers indicate 3-dB roll-off frequencies beyond 100 MHz.
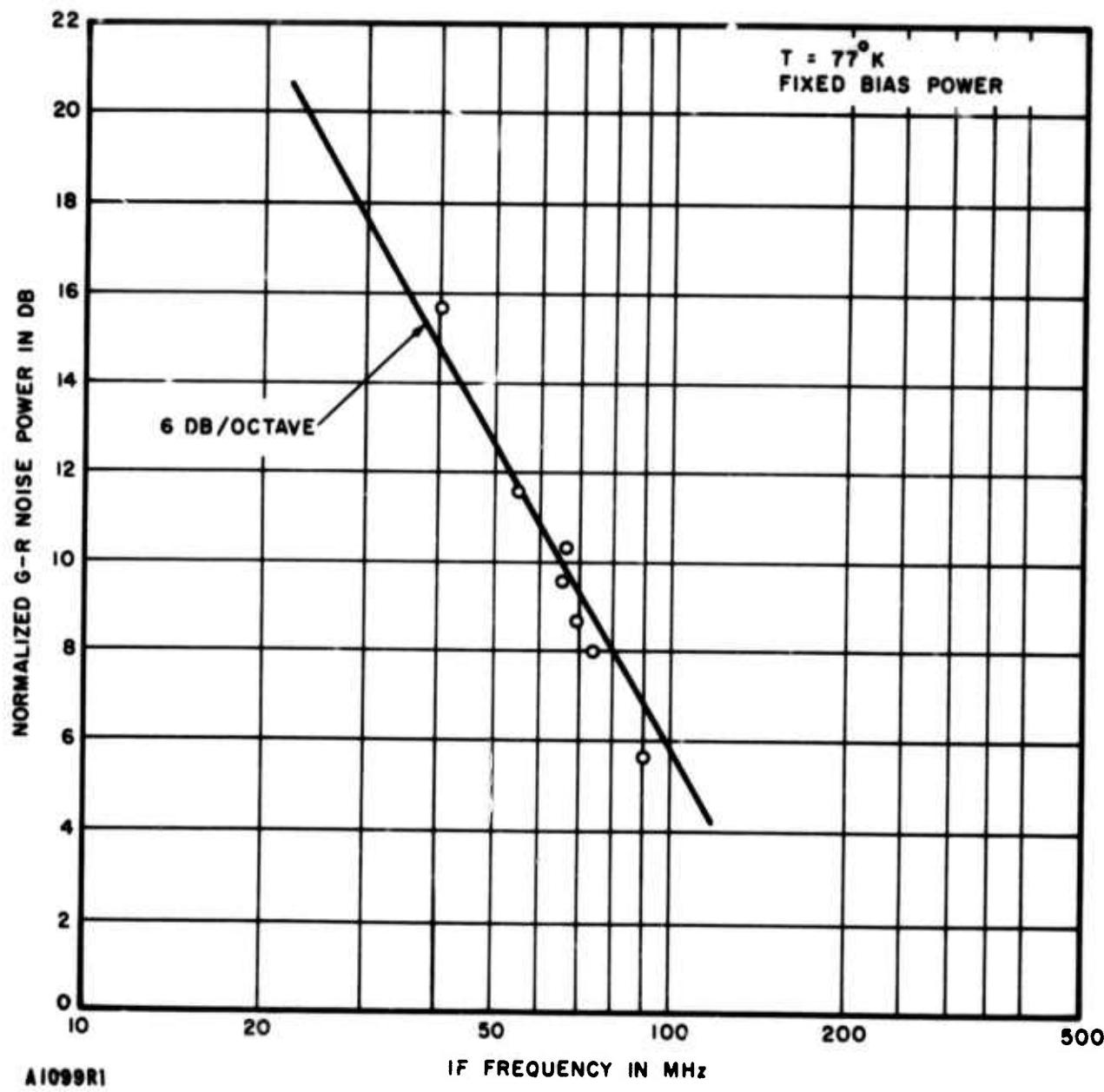
FIGURE 3-11. MEASURED G-R NOISE POWER FOR HgCdTe DETECTOR

Figure 3-12 shows the variation of the I-V characteristic of the HgCdTe mixer with LO power. The mixer resistance is seen to vary from 400 to 20 ohms when LO power is applied.

45
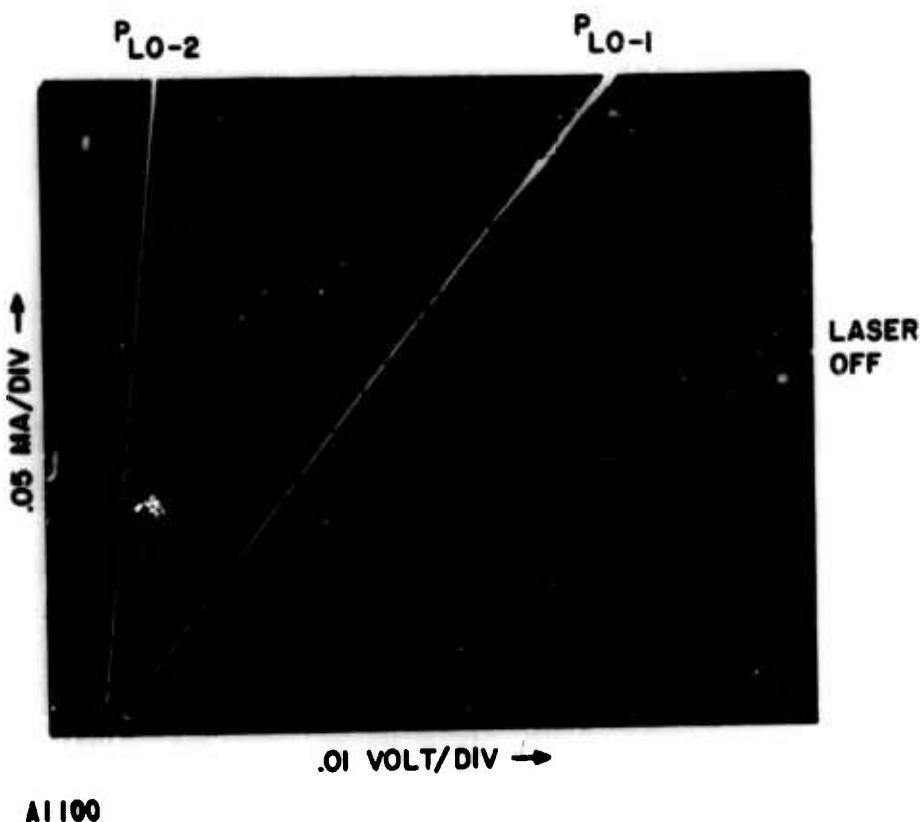
FIGURE 3-12. VARIATIONS OF RESISTANCE WITH LO POWER OF HgCdTe MIXER

H. IF AMPLIFIER

A prime objective of the amplifier design is the achievement of low noise, flat gain, and uniform input impedance broadband over the entire 10-MHz to 1.5-GHz band, in a single amplifier. Starting with an earlier 1-GHz amplifier design (reference 3) several modifications were tried. Results on the final model are given here. With the amplifier from a 50-ohm source, its gain was measured as a function of frequency and is given in Figure 3-13. The net gain is 38 dB in midband, and over 30 dB from 8 MHz to 1.4 GHz. The measured noise-factor of the amplifier is given in Figure 3-14. The midband value is 4.5 dB, increases to 6 dB at 1.1 GHz, and becomes 7.4 dB at 1.4 GHz. Work was carried out to extend the amplifier performance sufficiently beyond 1.5 GHz to assure satisfactory performance throughout the specified mixer operating band.

46
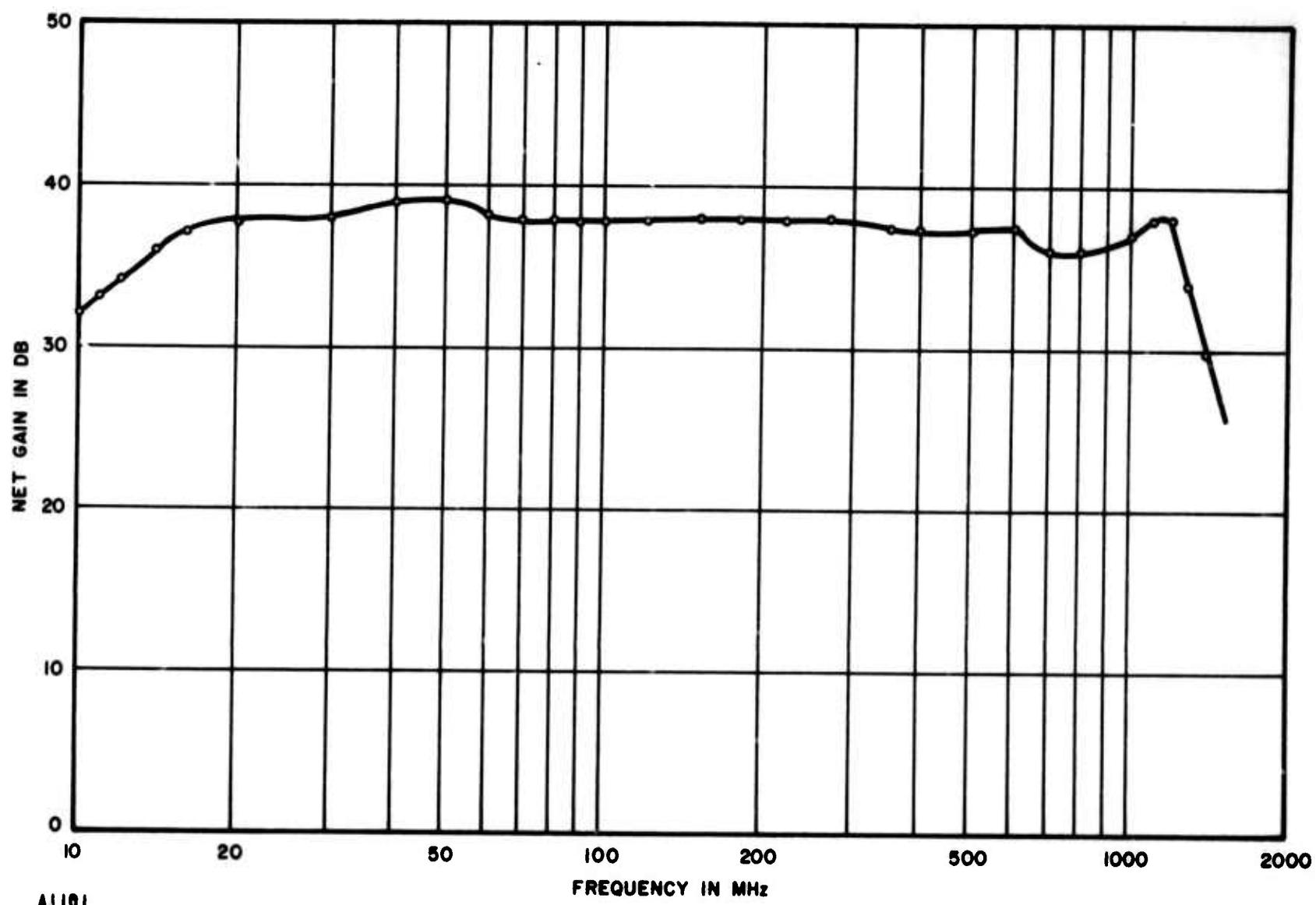
FIGURE 3-13. MEASURED NET GAIN OF WIDEBAND IF AMPLIFIER OPERATING FROM 50-OHM SOURCE RESISTANCE

This amplifier has been used in the evaluation of most of the mixer elements reported above and operated satisfactorily. A very useful feature of the amplifier was a matching transformer at its input that permitted the introduction of dc bias to the mixer element without the need for a broadband bias tee external to it. This transformer also provided a means for obtaining a better impedance match with the mixer element.

47
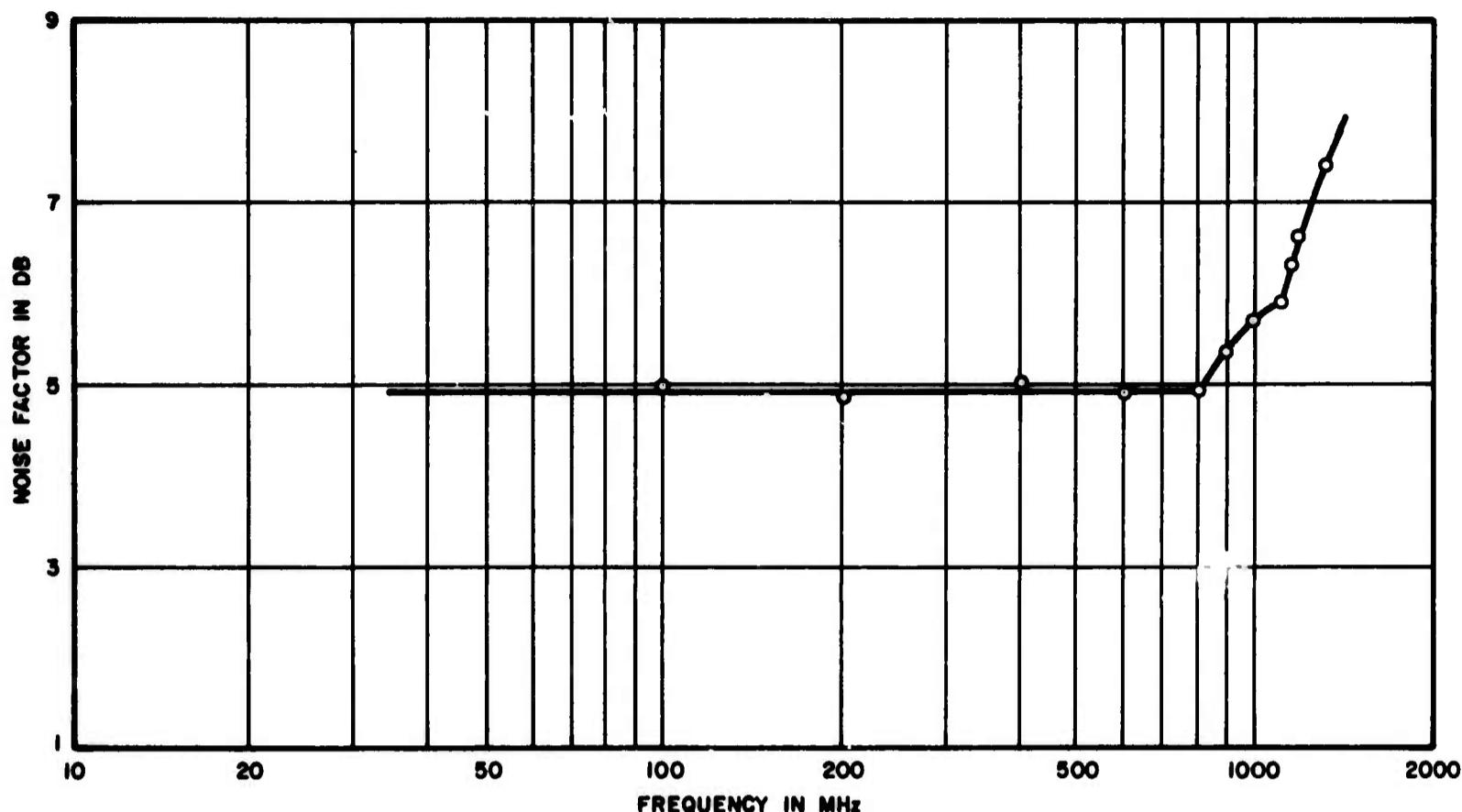
FIGURE 3-14. MEASURED NOISE FACTOR OF WIDEBAND IF AMPLIFIER OPERATING FROM 50-OHM SOURCE RESISTANCE

I. HIGHER-TEMPERATURE MIXER OPERATION

Higher temperature operation of the higher speed detectors developed on this program would permit the use of compact, reliable, closed-cycle coolers that have recently become available. Closed-cycle cooling not only eliminates the handling of cryogenic liquids but also accommodates the higher power dissipation of larger mixer arrays.

Measurements of high-frequency response have been made using an available closed-cycle cooler. The results obtained are given in Figure 3-15. As shown, good mixer noise performance was obtained out to 1200 MHz. This data is very encouraging since the setup was not optimized and insufficient local oscillator power was available.

48

5099
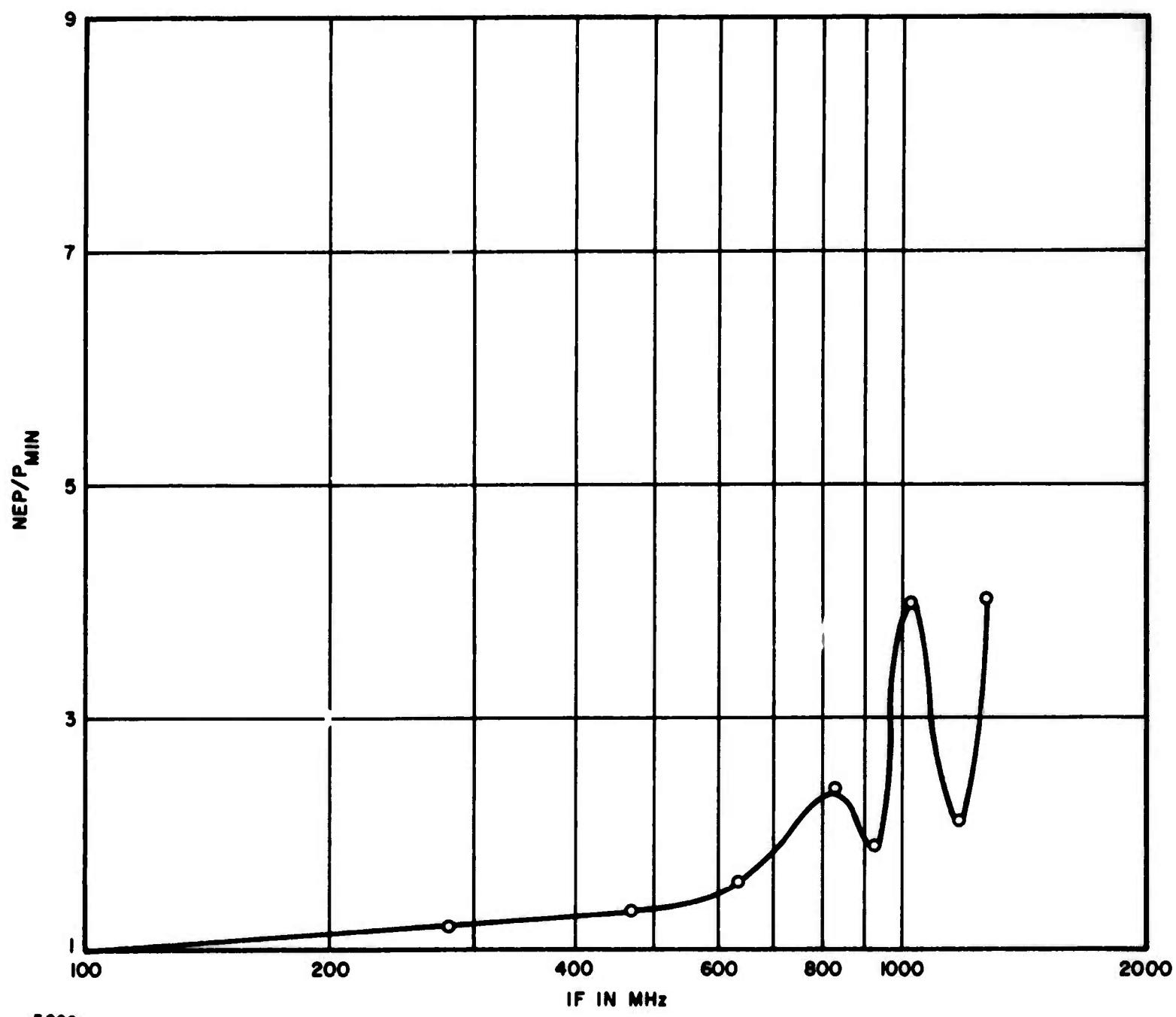
FIGURE 3-15. MEASURED FREQUENCY RESPONSE OF Ge:Cu MIXER AT RELATIVELY
HIGH TEMPERATURE IN CLOSED-CYCLE COOLER

IV. ARRAY FEASIBILITY DEMONSTRATION

A. ELECTRICAL CROSSTALK MEASUREMENTS

The high-frequency crosstalk between adjacent mixer elements in the array was measured under simulated operating conditions. With the mixer elements cooled to 4.2 K two sets of data were taken: one with both of the elements at their dark impedance level (about 900 kilohms), and the other measurement with the excited element irradiated by the laser local oscillator so that its impedance dropped to 2 kilohms. After some discussion it was concluded that these cases separately maximized the electric field coupling and the magnetic field coupling so that the worst case to be expected is included in these measurements. The mixer elements themselves are almost completely enclosed by the conducting copper structure. The crosstalk coupling was expected to occur at the parallel portion of the micro-strip fanout. Some unpublished measurements made at AIL on 50-ohm terminated lines of this type with microwave excitation indicated that -30 dB (order of magnitude) should be expected.

The data measured is shown in Figure 4-1. The upper curve was for both mixers in their high impedance conditions. The lower curve was for the excited mixer at 2 kilohms. The data out to 1 GHz indicates that no problem exists (-48 dB coupling). A pessimistic extrapolation out to 1.5 GHz might give -30 dB coupling. Since the optical side lobes are of the order of -16 dB, at this stage of development, the electrical crosstalk is expected to be of negligible importance. Should future developments result in a decrease in optical crosstalk it may become necessary to reduce the electrical crosstalk below present values. This can be done by introducing additional grounded strips between the present ones and can readily be done when required.

51
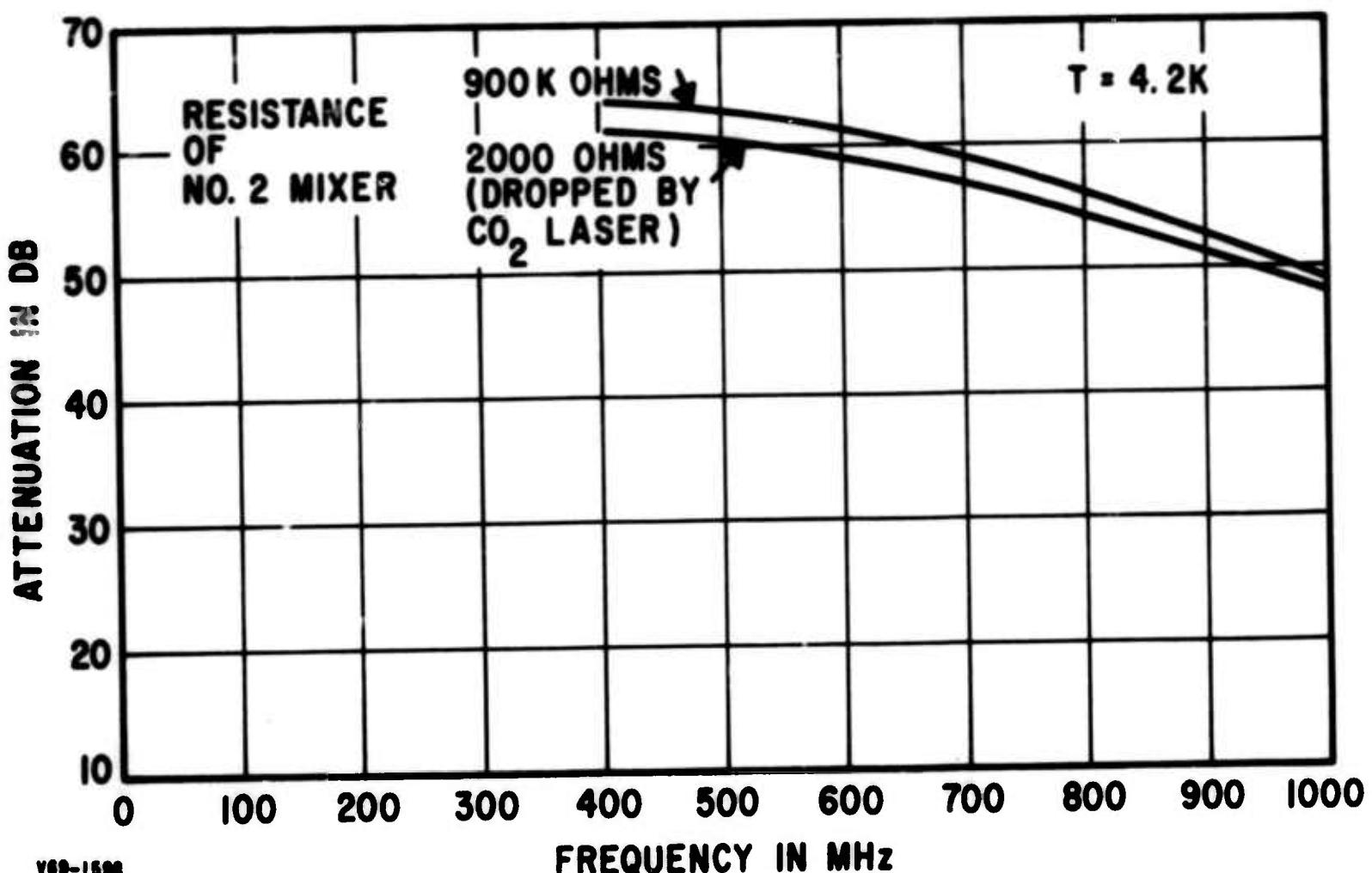
FIGURE 4-1. MEASURED DATA FOR ELECTRICAL CROSSTALK

B. OVERALL ARRAY PATTERNS

In this set of measurements the microlens array was mated with the array of infrared mixes and the overall receiving patterns were recorded. Each microlens was aligned with its corresponding mixer element and the whole unit was mounted to the cold plate inside the vacuum chamber of a liquid helium dewar. With the assembly at liquid helium temperature, the receiving pattern (IF component only) of each mixer element was measured. The oscilloscope photograph of Figure 4-2 is an automatically recorded trace in which the angle of arrival of the incoming signal was rapidly scanned across the mixer under test and its output signal displayed.

O-1822
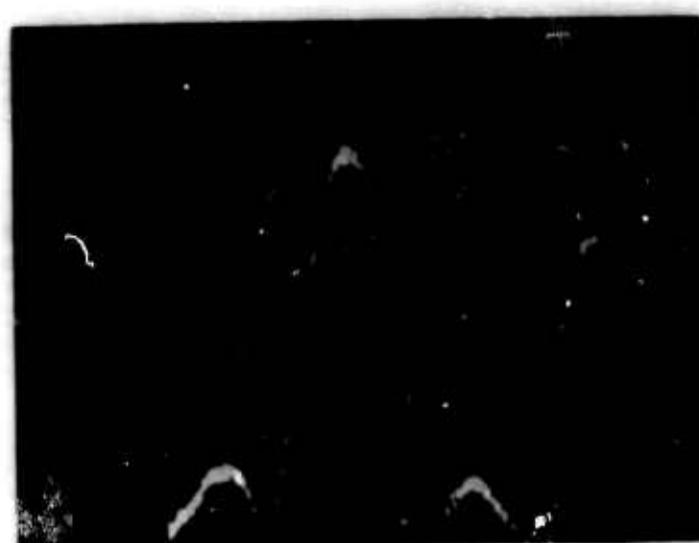
FIGURE 4-2. SCOPE TRACE OF OVERALL RECEIVING PATTERN FOR SINGLE ELEMENT

The individual receiving pattern is a multiplicative combination of the diffraction patterns of the circular aperture of the objective lens and the square apertures presented by the microlens and the mixer element itself. Since both the microlens and the mixer element are considerably smaller than the objective lens their radiation patterns are relatively broad so that the combined pattern will resemble the $J_1(x)/x$ pattern of the circular objective. The patterns of Section II illustrate this situation, especially that of Figure 2-2D in which the ratio of mixer size to spot size is close to the ratio of microlens size to spot size in the array. In addition, pattern modification results from central obscuration at the objective and dissection of the reference local oscillator beam.

A comparison of the measured scope photo and the computed curve of Figure 2-2D shows that the measured curve has higher and wider side lobes referred to its main lobe. This effect is attributable to the central obscuration of the objective lens in the measuring setup.

The receiving patterns of three adjacent mixer elements were measured and are shown in Figure 4-3 in registration with one another. The characteristics of these curves are similar to that of Figure 4-2 and the same comments apply. These patterns crossover at 3.1 dB and 3.0 dB below the central peak. The design value was 3.0 dB. This represents the achievement of prime objective of the program, that is, 3-dB crossovers with mixer elements under the operating conditions of local oscillator and cooling.

53
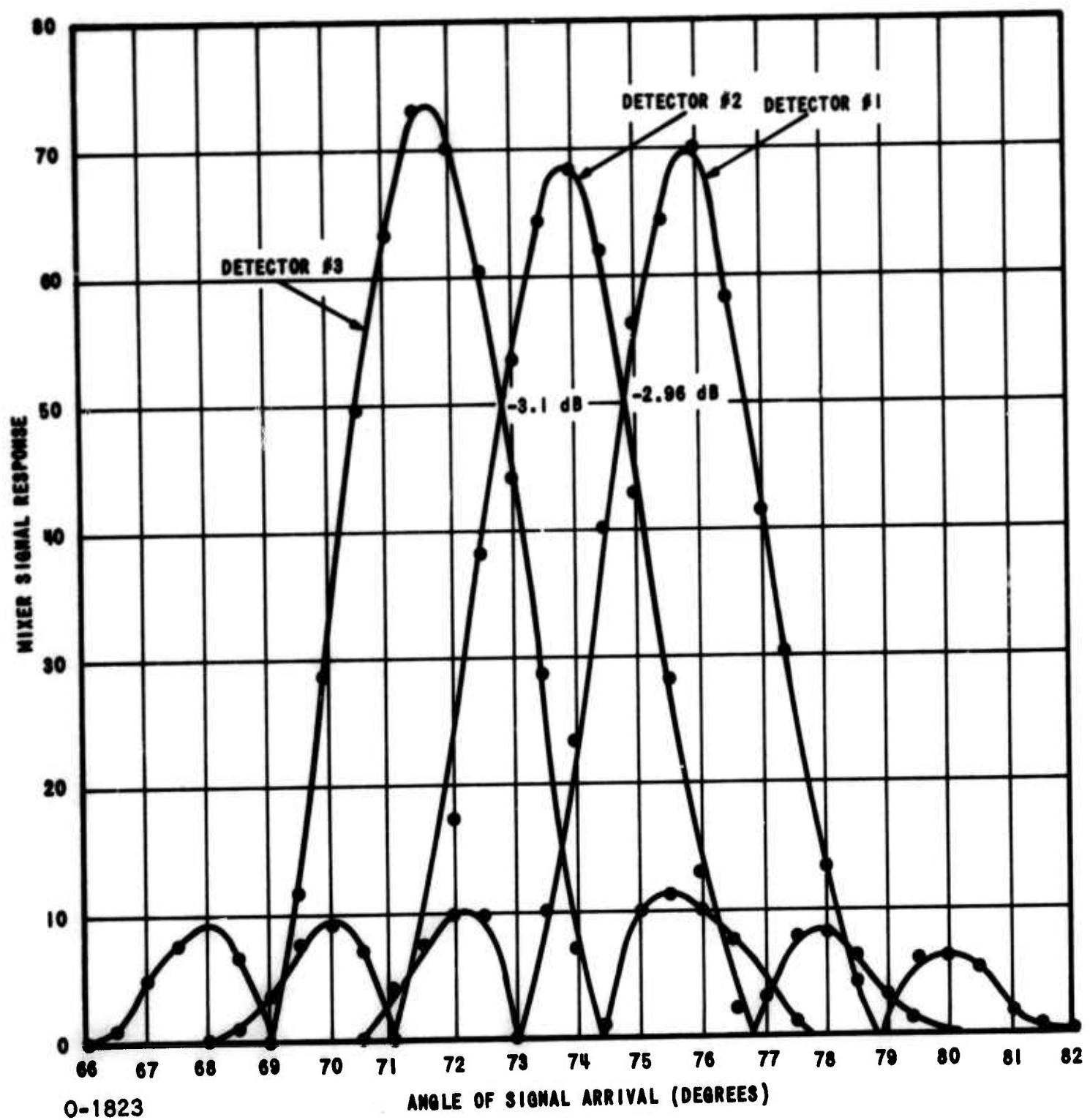
FIGURE 4-3. RECEIVING PATTERNS OF OVERALL SYSTEM FOR THREE ADJACENT MIXER ELEMENTS

54

V. SUMMARY AND CONCLUSIONS

This program has met its objectives by demonstrating:

- A structure to support a 3 × 3 configuration of high-performance 10.6-micrometer mixer elements

- An array of microlenses that generate receiving antenna beams in registration and crossing each other at a point 3 dB below their peak responses

- A mixer-preamplifier combination with measured NEP values of better than 2×10^{-19} watts/Hz from 10 MHz to 1500 MHz

- A microstrip cabling technique to handle the microwave IF signals detected by the infrared mixers

- Adequate thermal conductivity in the array structure to extract heat dissipated by the local oscillator beam and dc bias current

- At least 30 dB of electrical isolation at 1500 MHz between adjacent cooled mixer elements

In addition to meeting the program objectives the technology developed here is clearly extendable to larger arrays of up to and possibly beyond 10 × 10 mixer elements.

VI. REFERENCES

1. F. Pace, F. Arams, R. Lange, B. Peyton, E. Sard, and J. Ramsay, "Advanced Capability Infrared Receiver System, First Semiannual Progress Report," AIL Report 3481-I-1, October 1968.

2. F. Arams, E. Sard, B. Peyton, and F. Pace, "Infrared 10.6-Micron Heterodyne Detection with Gigahertz IF Capability," IEEE Journal of Quantum Electronics, Vol QE-3, p 484-492, November 1967.

3. F. Arams, B. Peyton, F. Pace, and R. Lange, "Packaged Infrared 10.6-Micron Heterodyne 1-GHz Bandwidth Receiver," Digest of the Electron Devices Meeting, Washington, D. C., October 1968.

4. "High-Sensitivity Infrared (10.6 Micron) Heterodyne Receivers with Gigahertz IF Capability Part I. Sensitivity and Bandwidth; Part II Receiver Development," IEEE Spectrum, Vol 5, p 5, June and July 1968.

5. R. A. Soref, "Extrinsic Infrared Photoconductivity of Si Doped with B, Al, Ga, As, or Sb," Journal of Applied Physics, December 1967.

6. G. A. Korn and T. A. Korn, Mathematical Handbooks for Scientists and Engineers, Section 21.8, McGraw-Hill, New York, 1961.

A-1 S. Silver, Microwave Antenna Theory and Design, MIT Radiation Laboratory Series, Vol 12, Chapter 6, McGraw-Hill, New York, 1949.

A-2 G. W. Stroke, "Diffraction Gratings," Handbuch der Physik, S. Flugge, ed., Vol XXIX, Springer, Berlin, 1968.

B-1 M. DiDomenico and O. Svelto, "Solid-State Photodetection: A Comparison between Photodiodes and Photoconductors," Proc IEEE, February 1959.

B-2 G. Lucovsky, M. E. Lasser, and R. B. Emmons, "Coherent Light Detection in Solid-State Photodiodes," Proc IEEE, Vol 51, p 166, January 1963.

B-3 L. K. Anderson, "Measurement of the Microwave Modulation Frequency Response of Junction Photodiodes," Proc IEEE, May 1963.

APPENDIX A

DERIVATION OF FIELD PATTERNS FOR IF COMPONENT AND MIXED SIGNAL

Consider, first, the received signal that is focused by the receiving aperture onto the image plane within the coordinate system defined in Figure A-1. The incoming signal propagates in the direction given by:
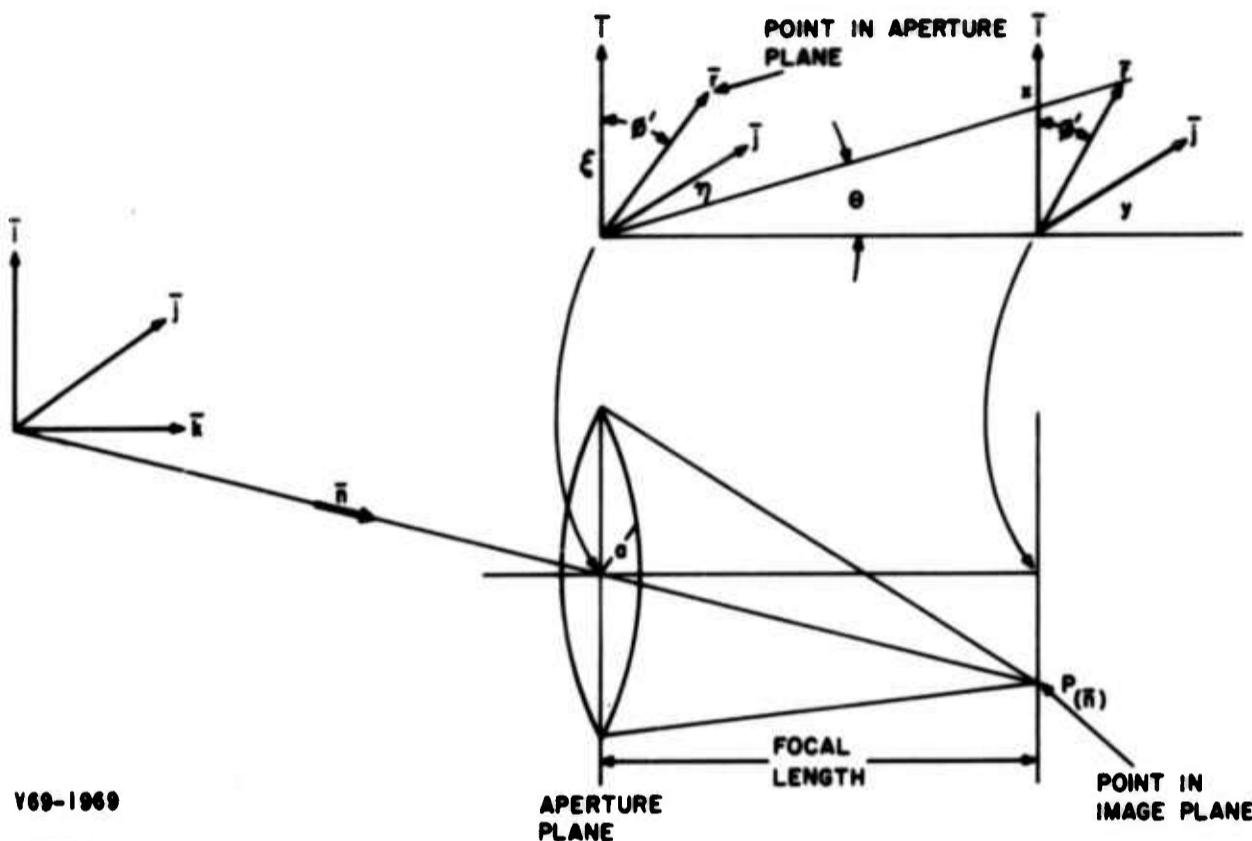
FIGURE A-1. COORDINATES FOR HETERODYNE RECEIVER BEAM PATTERN ANALYSIS

$$\overline{n} = \overline{i}\alpha' + \overline{j}\beta' + \overline{k}\gamma'$$

where

$\overline{i}, \overline{j}, \overline{k}$ = unit vectors for the rectangular coordinate system

α', β', γ' = direction cosines, and any point in the aperture plane is

$$\overline{r} = \overline{i}\xi + \overline{j}\eta$$

where ξ, η = aperture plane coordinates.

Under certain conditions, the field at the receiving aperture is related to the field at the image plane by the Fourier transformation. The expression for this transformation is derived by Silver and also by Stroke (references A-1, A-2). According to Stroke, three important approximations to the rigorous electromagnetic wave treatment of this field vector problem are involved in the derivation of the Fourier integral representation of the Fraunhofer region. This representation applies to:

1. Center and near-vicinity of a quasispherical wavefront of radius R

2. Values of wavelength $\lambda \ll R$

3. a) Electromagnetic field vectors $\overline{E}$ and $\overline{H}$ which are tangent to the wavefront

   b) $\overline{E}$, $\overline{H}$, and the gradient of the wavefront, which form an orthogonal triad

Condition 1 refers to that region where small angle approximations are valid; that is, the case of interest here. Condition 2 certainly met at infrared wavelengths. Condition 3 is met for high f/number systems in that, in such a case, the bundle of rays converges slowly to a focus. It has been shown that an f/number greater than four ensures the validity of the scalar approximation of the vector treatment of electromagnetic wave interactions at the focus of a lens.

Stroke's formulation of the Fourier integral representation is given as:

$$\overline{E}_p(k\alpha,\ k\beta) = \frac{i}{\lambda}\frac{e^{-ikf}}{f}\int\limits_{\xi}\int\limits_{\eta} \overline{E}_o\, e^{ik\,\Delta(\xi,\ \eta)}\, e^{ik(\alpha\xi\ +\ \beta\eta)}\, d\xi d\eta$$

$$\text{aperture plane}$$

where

$\overline{E}_p(k\alpha,\ k\beta)$ = complex amplitude of the electric field vector at a point (P), in the image plane, with coordinate values $(k\alpha,\ k\beta)$,

$k = 2\pi/\lambda$,

λ = wavelength,

$(k\alpha,\ k\beta)$ = image plane coordinates expressed in terms of the direction cosines of plane waves incident on the receiving aperture,

$i = \sqrt{-1}$,

f = focal length of lens,

$(\xi,\ \eta)$ = rectangular coordinates of aperture plane,

$\bar{E}_0 = E_T e^{-i\omega_T t}$ = complex amplitude of the electric field, in the aperture plane, with sinusoidal time variation ω_T.

The phase variation over the aperture, with respect to the coordinate origin, is given by:

$$\Delta = k\ \bar{r} \cdot \bar{n} = k(\xi\alpha' + \eta\beta')$$

For the paraxial case, where $\bar{n}$ is at only small angles to the optic axis:

$$\alpha' \cong \frac{x'}{f} \text{ and } \beta' \cong \frac{y'}{f}$$

likewise

$$\alpha \cong \frac{x}{f} \text{ and } \beta \cong \frac{y}{f}$$

For a uniform plane wave incident from direction $\bar{n}$, E_T is constant and Δ is as given. This reduces the integral to the form:

$$I_0 = \int_\xi \int_\eta e^{i\frac{k}{f}[(x+x')\xi + (y+y')\beta]}\ d\xi d\eta$$

For a circular aperture let

$$\xi = \rho \cos \phi'$$

$$\eta = \rho \sin \phi'$$

$$\rho = \left(\xi^2 + \eta^2\right)^{1/2}$$

where ϕ' is defined in Figure A-1. With this substitution

$$I_0 = \int_0^a \int_0^{2\pi} e^{\frac{ik\rho}{f}[(x+x')\cos\phi' + (y+y')\sin\phi']} \rho \, d\phi' \, d\rho$$

and substituting

$$A = \frac{k\rho}{f}\left[\left(x + x'\right)^2 + \left(y + y'\right)^2\right]^{1/2}$$

$$\psi = \arctan\frac{(x + x')}{(y + y')}$$

gives

$$I_0 = \int_0^a \rho\left[\int_0^{2\pi} e^{iA\sin(\phi'+\psi)} \, d\phi'\right] d\rho$$

the inner integral (I_1) may be expanded into Bessel functions by means of the Jacobi-Anger formula (reference 6) into

$$I_1 = \int_0^{2\pi} J_0(A) + 2\sum_{k=1}^{\infty}\left\{J_{2k}(A)\cos\left[2k(\phi' + \psi)\right] + iJ_{2k-1}(A)\sin\left[(2k - 1)(\phi' + \psi)\right]\right\} d\phi'$$

Integrating gives 2π for the first term and zero for both the sine and cosine terms; therefore,

$$I_0 = 2\pi \int_0^a \rho J_0\left\{\frac{k\rho}{f}\left[\left(x + x'\right)^2 + \left(y + y'\right)^2\right]^{1/2}\right\} d\rho$$

Integrating, by means of Lommel's Integral (reference 6), gives

$$I_0 = 2\pi a^2 \frac{J_1\left\{\frac{ka}{f}\left[\left(x+x'\right)^2 + \left(y+y'\right)^2\right]^{1/2}\right\}}{\frac{ka}{f}\left[\left(x+x'\right)^2 + \left(y+y'\right)^2\right]^{1/2}}$$

This expression gives (within a multiplicative constant) the electric field distribution in the image plane (x,y), in terms of the direction of arrival (α', β') of a plane wave incident on the receiving aperture. Where (α', β') are referred to the image plane (x', y') by the previous equations. The expression describes a diffraction field of the form

$$\frac{J_1(X)}{X}$$

in two dimensions, with center displaced off-axis to a new origin $(-x', -y')$.

Consider, now, the local oscillator beam which is incident on the image plane from a direction

$$\bar{n} = \bar{i}\epsilon + \bar{j}\delta + \bar{k}\mu$$

Again, defining a reference vector $(\bar{r}')$ in the image plane as $\bar{r}' = \bar{i}x + \bar{j}y$, and the phase difference over the image plane as

$$\Delta' = k\bar{r}' \cdot \bar{n}' = k(\epsilon x + \delta y)$$

Therefore, the field at the image plane, due to the local oscillator, may be represented by

$$\bar{E}_{LO}(x, y) = E_{LO}\, e^{-i\omega_0 t}\, e^{ik(\epsilon x + \delta y)}$$

The fields of the received signal, and the local oscillator at the image plane (the mixer is placed here), are now combined by addition (again assuming that the polarizations of the two components are aligned) and the intensity of the resultant computed:

$$I_i = \left\langle \left(E_{LO} + E_p \right)^2 \right\rangle \, \frac{1}{2T} \int_{-T}^{T} \left(E_{LO}^2 + E_p^2 + E_{LO}\, E_p^* + E_{LO}^*\, E_p \right) dt$$

The period of integration (2T) is taken very long compared to the period of the infrared frequency, but short compared to the period of the frequency difference introduced by the two cross terms. Therefore, the first two terms in the integrand result in dc outputs from the mixer and are of no interest at this point. The two cross terms result in the intermediate (IF) signal. The mixer responds to the real parts of these last two terms and it can be shown by direct substitution that

$$R_e \left(E_{LO}\, E_p^* \right) = \left(E_{LO}^*\, E_p \right)$$

so that only one of these terms need be considered further. Moreover, the mixer responds to the integrated intensity, over its surface, so that the mixer output is given by

$$I_m = M \cdot 2 R_e \int_{\substack{mixer \\ area}} \left(E_{LO}\, E_p^* \right) dA$$

$$= \frac{M\, 2 a^2 k}{f} E_L\, E_T \int_{\substack{mixer \\ area}} \sin \left[\left(\omega_T - \omega_o \right) t + k \left(f + \epsilon x + \delta y \right) \right] \cdot$$

$$\frac{J_1 \left\{ \frac{ka}{f} \left[\left(x+x' \right)^2 + \left(y+y' \right)^2 \right]^{1/2} \right\}}{\frac{ka}{f} \left[\left(x+x' \right)^2 + \left(y+y' \right)^2 \right]^{1/2}} dA$$

where M is a proportionality constant relating the intensity at the mixer to the amplitudes of the IF signal output. Letting

$$C = \frac{M\, 2a^2\, k\, E_L\, E_T}{f}$$

and assuming a square mixer element, gives

64

$$I_m = C \int_{y_1-\Delta y}^{y_1+\Delta y} \int_{x_1-\Delta x}^{x_1+\Delta x} \sin\left[\left(\omega_T - \omega_0\right) t + kf + k(\epsilon x + \delta y)\right] \cdot$$

$$\frac{J_1\left\{\frac{ka}{f}\left[\left(x+x'\right)^2 + \left(y+y'\right)^2\right]^{1/2}\right\}}{\frac{ka}{f}\left[\left(x+x'\right)^2 + \left(y+y'\right)^2\right]^{1/2}} \, dx \, dy$$

where

(x_1, y_1) = coordinates of the center of the square mixer,

$(2\Delta x, 2\Delta y)$ = dimensions of the square mixer.

In this equation, the argument of the sine term consists of three parts. The first part is the time-varying component that produces the IF signal; the second part represents a fixed phase that can be dropped without loss of generality, so long as $(\omega_T - \omega_0)$ is not equal to zero; the third term gives a variation in spatial phase across the mixer, caused by tilt in the local oscillator phase wavefront with respect to the mixer surface. When the local oscillator propagation direction and the mixer surface normal coincide ($\epsilon = \delta = 0$) and the third term disappears.

The Bessel function term gives an intensity pattern that is similar to the Airy disc field pattern rather than the square of the field pattern. This is brought about by the linearizing effect of a high-level local oscillator field and selection of the resulting IF component, only.

The integral describing the IF signal output may be normalized by the following substitutions

$$X = \frac{ka}{f} x = \frac{\pi}{\lambda F} x$$

$$Y = \frac{ka}{f}\, y = \frac{\pi}{\lambda F}\, y$$

where $F = f/2a = f/\text{number}$ of the optical system to give

$$I_m = C \left(\frac{\lambda F}{\pi}\right)^2 \int_{\frac{\pi}{\lambda F}\left(Y_1-\Delta Y\right)}^{\frac{\pi}{\lambda F}\left(Y_1+\Delta Y\right)} \int_{\frac{\pi}{\lambda F}\left(X_1-\Delta X\right)}^{\frac{\pi}{\lambda F}\left(X_1+\Delta X\right)} \sin\left[\left(\omega_1 - \omega_o\right) t + 2F\left(\epsilon X + \delta Y\right)\right].$$

$$\frac{J_1\left\{\left[\left(X+X'\right)^2 + \left(Y+Y'\right)^2\right]^{1/2}\right\}}{\left[\left(X+X'\right)^2 + \left(Y+Y'\right)^2\right]^{1/2}}\, dX dY$$

In this form, it is apparent that the only characteristic of the optical system (within the limitations imposed by the assumptions used in the derivation) that affects the IF signal output is its f/number. The normalized coordinates (X, Y) represent the ratios of linear dimensions in the image plane to the spot diameter.

APPENDIX B

INFRARED PHOTOVOLTAIC MIXER ANALYSIS

1. INTRODUCTION

An analysis was carried out on the noise equivalent power and IF frequency band-width of infrared photovoltaic mixers, with emphasis on 10.6-micrometer mixing (in such diodes as PV-HgCdTe). Various formulas scattered throughout the literature (references B1 and B2) have been modified to obtain explicit formulas for mixer conversion gain, noise equiv-alent power (NEP) and IF bandwidth, in terms of such parameters as photodiode capacitance, shunt and series resistance, local oscillator power, etc. The use of double- and triple-tuned circuits to extend the high-frequency response was also investigated. The analysis employs the same conversion gain approach successfully used in the analysis of photoconductive mixers. The objective of the analysis was to gain insight into the potential of 1.5 GHz PV-mixer operation.

2. AVAILABLE IF SIGNAL POWER

The equivalent circuit at IF frequencies for a photovoltaic (PV) infrared mixer is shown in Figure B-1. The mixer analysis assumes a nonzero leakage conductance and neglects any lead inductance which may be present.

The square of the peak IF signal current is given by:

$$\left| I_S^2 \right| = 4 \left(\frac{\eta q}{h\nu} \right)^2 P_{sig} \, P_{LO}$$

where

I_S = peak IF signal current

ν = signal frequency

η = quantum efficiency
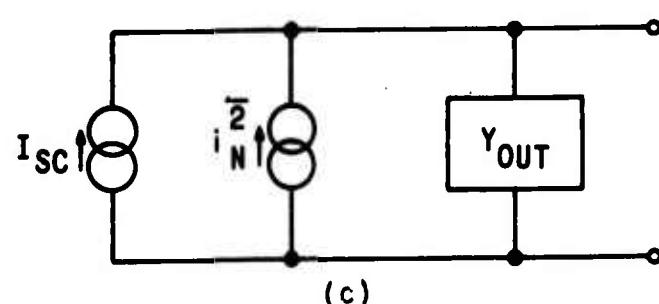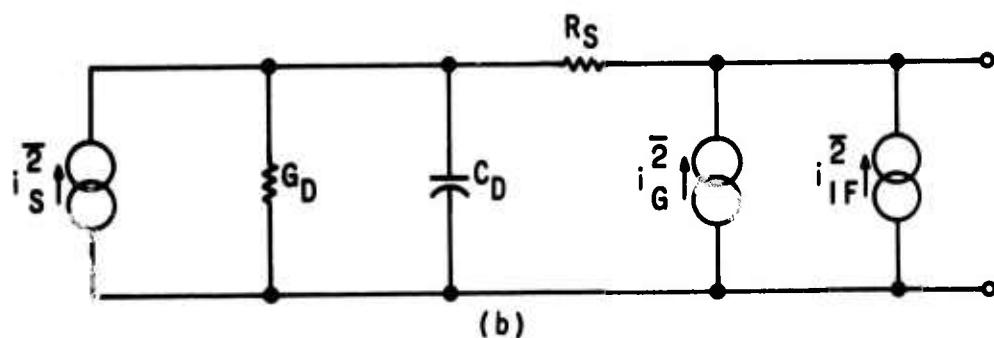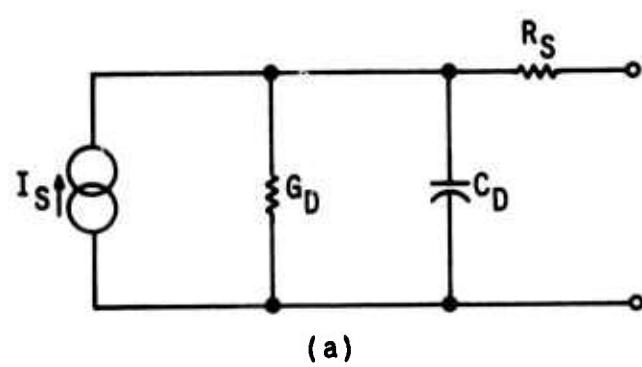
A1103
V69-1923

FIGURE B-1. EQUIVALENT CIRCUIT FOR INFRARED PHOTOVOLTAIC MIXER

P_{sig} = signal power

P_{LO} = LO power > P_{sig}

From Figure B-1, the ratio of the short circuit current to the signal current is given by:

$$\frac{I_{SC}}{I_S} = \frac{1}{\left(1 + G_D\, R_S\right) + j\omega\, C_D\, R_S}$$

where

I_{SC} = short circuit current

G_D = small signal shunt conductance (slope of I-V curve)

R_S = series resistance

C_D = shunt capacitance

The mixer output admittance can be expressed as:

$$Y_{out} = \frac{G_D + R_S\left(G_D^2 + \omega^2\, C_D^2\right) + j\omega\, C_D}{\left(1 + G_D\, R_S\right)^2 + \omega^2\, C_D^2\, R_S^2}$$

The real component of the output admittance is given by

$$G'_{out} = \frac{G_D + R_S\left(G_D^2 + \omega^2\, C_D^2\right)}{\left(1 + G_D\, R_S\right)^2 + \left(f/f_c\right)^2}$$

where the cutoff frequency f_c is defined as

$$f_c = \frac{1}{2\pi\, R_S\, C_D}$$

For most photovoltaic mixer elements $G_D\, R_S \ll 1$, so that

69

$$G'_{out} \approx \frac{G_D + \omega^2 C_D^2 R_S}{1 + \left(f/f_c\right)^2}$$

The squared short-circuit current is:

$$\left|I_{SC}\right|^2 = \frac{\left|I_S\right|^2}{\left(1 + G_D R_S\right)^2 + \left(f/f_c\right)^2}$$

and the available output power from the photovoltaic mixer is:

$$\left(P_{IF}\right)_{available} = \frac{\left|I_{SC}\right|^2}{8\,G'_{out}} = \frac{\left|I_S\right|^2}{8\left[G_D\left(1 + G_D R_S\right) + \omega^2 R_S C_D^2\right]}$$

The output power is 3 dB down at an IF frequency given by:

$$f'_c = \frac{\left(1 + R_S G_D\right)^{1/2}}{2\pi C_D \left(R_{S/G_D}\right)^{1/2}} \approx \frac{1}{2\pi C_D \left(R_{S/G_D}\right)^{1/2}}$$

3.   NOISE

The equivalent noise circuit for the photovoltaic mixing case including noise generators is shown in Figure B-2. The overall mean-square noise current generator is given by:

$$\overline{i_N^2} = \overline{i_G^2} + \overline{i_{IF}^2} + \frac{\overline{i_S^2}}{\left(1 + G_S R_S\right)^2 + \left(f/f_c\right)^2}$$

70

where

$$\overline{i_G^2} = \text{thermal noise} = 4RT_m B\, G'_{out}$$

$$\overline{i_{IF}^2} = \text{IF amplifier noise} = 4RT'_{IF} B\, G'_{out}$$

$$\overline{i_S^2} = \text{shot noise} \approx 2q\, I_0 B \text{ for condition } f_{IF} < 1/(8T_r) \text{ (reference B-3)}$$

k = Boltzmann's constant

T_m = physical temperature of mixer

B = IF bandwidth

T'_{IF} = effective input noise temperature of IF amplifier which is a function of its source impedance

I_0 = dc photocurrent

T_r = carrier transit time

A1104
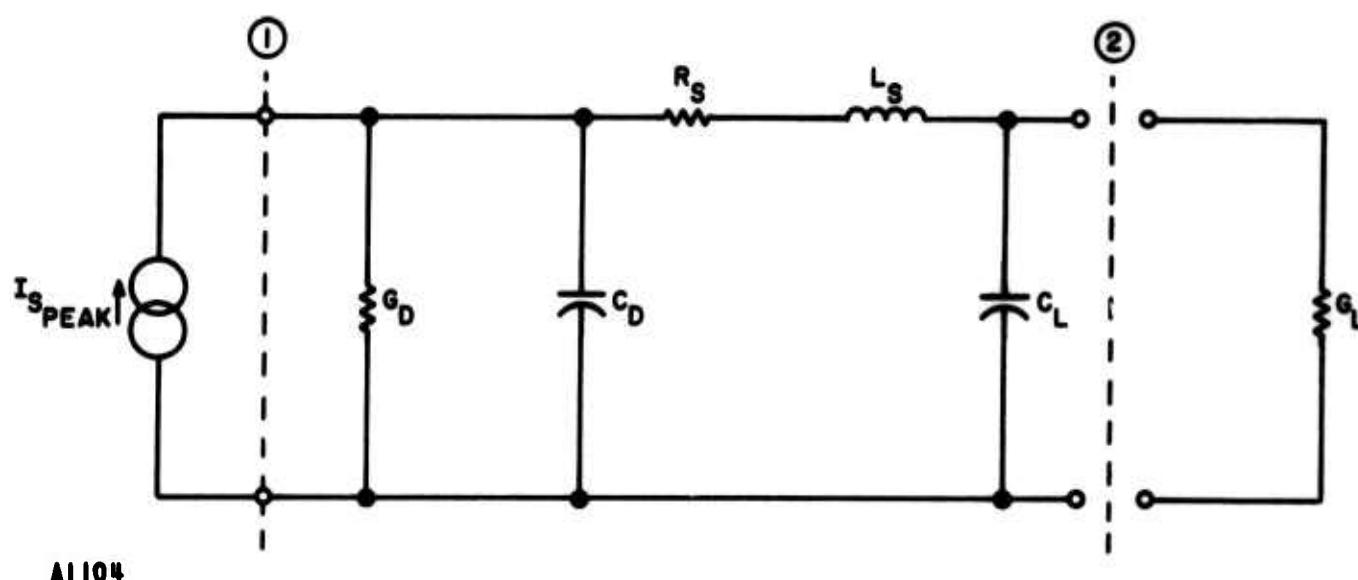
FIGURE B-2. EQUIVALENT CIRCUIT FOR TUNED PHOTOVOLTAIC MIXER

4. MIXER GAIN

The available photovoltaic mixing gain--that is, the ratio of the available IF output power to the available infrared signal power, is given by:

$$G = \frac{P_{IF \ (available)}}{P_{sig}} = \frac{\left| I_S \right|^2}{8 \, P_{sig} \left[G_D \left(1 + G_D \, R_S \right) + \omega^2 \, R_S \, C_d^2 \right]}$$

which can be written as

$$G = \frac{\left(\frac{\eta q}{h\nu} \right)^2 P_{LO}}{2 \left[G_D \left(1 + G_D \, R_S \right) + \omega^2 \, R_S \, C_d^2 \right]}$$

For photovoltaic mixer $\tau / T_r = 1$. Therefore (reference 2), under the condition that, $P_{LO} >> P_{sig}$, the dc photocurrent is given by:

$$I_0 = \frac{\eta q}{h\nu} \left(\frac{\tau}{T_r} \right) P_{LO} = \frac{q}{h\nu} \eta \, P_{LO}$$

Combining these equations:

$$G = \frac{\eta q I_0}{2h\nu} \frac{1}{G_D \left(1 + R_S \, G_D \right) + \omega^2 \, R_S \, C_D^2}$$

and for $R_S \, G_D << 1$

$$G \approx \frac{\eta q I_0}{2 \, h\nu \, G_D} \frac{1}{1 + \left(f / f_c' \right)^2}$$

From this, is seen that the available conversion gain is 3 dB down at an IF frequency $\left(f_c' \right)$ defined above.

72

It is interesting to note that the conversion gain varies with LO power through its effect on the photocurrent, I_o.

5. SIGNAL-TO-NOISE RATIO

The signal-to-noise ratio for the photovoltaic mixer is:

$$\frac{S}{N} = \frac{\left| I_{SC} \right|^2}{2 \, \overline{i_N^2}}$$

Substituting expressions for the noise current and the short circuit current given:

$$\frac{S}{N} = \frac{\left| I_S \right|^2}{8k \left(T_m + T_{IF}' \right) B \left[G_D + R_S \left(G_D^2 + \omega^2 C_D^2 \right) \right] + 4q I_o B}$$

$$= \frac{\left(\frac{\eta q}{h\nu} \right) P_{sig} \, I_o}{I_o q B + 2k \left(T_m + T_{IF}' \right) B \left[G_D \left(1 + R_S G_D \right) + \omega^2 R_S C_D^2 \right]}$$

Thus, the noise equivalent power (NEP), that is, the value of signal power to give an IF signal-to-noise ratio equal to unity, is:

$$NEP = \frac{h\nu B}{\eta} \left\{ 1 + \frac{2k \left(T_m + T_{IF}' \right)}{q I_o} \left[G_D \left(1 + R_S G_D \right) + \omega^2 R_S C_D^2 \right] \right\}$$

This is reducible to:

$$NEP = \frac{h\nu B}{\eta} + \frac{k \left(T_m + T_{IF}' \right) B}{G}$$

which is the same expression as that derived for the photoconductive mixing case, with the exception of the factor of two in the quantum noise term due to the generation recombination

noise in photoconductors. Moreover, there are differences in the expressions for G, the conversion gain, between photovoltaic and photoconductive mixing.

6. QUANTUM NOISE FACTOR

The quantum noise factor is defined as the noise equivalent power divided by the fundamental limiting quantum power ($h\nu B$):

$$QF = \frac{1}{\eta}\left[1 + \frac{R\left(T_m + T'_{IF}\right)}{h\nu G}\right]$$

DOCUMENT CONTROL DATA - R & D

(Security classification of title, body of abstract and indexing annotation must be entered when the overall report is classified)

1. ORIGINATING ACTIVITY *(Corporate author)*	2a. REPORT SECURITY CLASSIFICATION
AIL, a division of Cutler-Hammer Deer Park, New York 11729	**UNCLASSIFIED**
	2b. GROUP

3. REPORT TITLE

ADVANCED CAPABILITY INFRARED RECEIVER SYSTEM

4. DESCRIPTIVE NOTES *(Type of report and inclusive dates)*

Final Report (15 March 1968 to 15 December 1969)

5. AUTHOR(S) *(First name, middle initial, last name)*

F. Pace, R. Lange, F. Arams, B. Peyton, and E. Sard

6. REPORT DATE	7a. TOTAL NO. OF PAGES	7b. NO. OF REFS
March 1970	78	11

8a. CONTRACT OR GRANT NO.	9a. ORIGINATOR'S REPORT NUMBER(S)
N00014-68-C-0273	
b. PROJECT NO. 7E20K21	AIL Report 3481-F
c. ARPA Order No. 306	9b. OTHER REPORT NO(S) *(Any other numbers that may be assigned this report)*
d.	

10. DISTRIBUTION STATEMENT

Reproduction in whole, or in part, is permitted for any purpose of the United States Government.

11. SUPPLEMENTARY NOTES This research is part of Project DEFENDER under the joint sponsorship of the Advanced Research Project Agency, the Office of Naval Research, and the DOD.	12. SPONSORING MILITARY ACTIVITY Office of Naval Research

13. ABSTRACT This is the final report on a program that has demonstrated the following technological achievements:

- A structure to support a 3×3 configuration of high performance 10.6 micrometer mixer elements.
- An array of microlenses that generate receiving antenna beams in registration and crossing each other at a point 3 dB below their peak responses.
- A mixer-preamplifier combination with measured NEP values of better than 2×10^{-19} watts/Hz from 10 MHz to 1500 MHz.
- A microstrip cabling technique to handle the microwave IF signals detected by the infrared mixers.
- Adequate thermal conductivity in the array structure to extract the heat dissipated by the local oscillator beam and dc bias current.
- At least 30 dB of electrical isolation at 1500 MHz between adjacent cooled mixer elements.

   In addition to meeting the program objectives the technology developed here is clearly extendable to larger arrays of up to and possibly beyond 10×10 mixer elements.

DD FORM 1473

14. KEY WORDS	LINK A		LINK B		LINK C	
	ROLE	WT	ROLE	WT	ROLE	WT
Antenna Patterns						
Coherent Array						
CO_2 Lasers						
Infrared Mixer						
Photovoltaic Mixer						
10.6 Micron Mixer						

KEY WORDS	LINK A		LINK B		LINK C	
	ROLE	WT	ROLE	WT	ROLE	WT